Applied Materials Today 35 (2023) 101937

Contents lists available at ScienceDirect

Applied Materials Today

journal homepage: www.elsevier.com/locate/apmt

Polymer materials as catalysts for medical, environmental, and energy applications

Federico Mazur, Andy-Hoai Pham, Rona Chandrawati *

School of Chemical Engineering and Australian Centre for Nanomedicine (ACN), The University of New South Wales, Sydney, NSW 2052, Australia

ARTICLE INFO

Keywords:
Catalytic polymeric materials
Photocatalysis
Graphitic carbon nitride
Covalent organic frameworks

ABSTRACT

Catalysts are the backbone of almost all aspects in life, increasing the rate of chemical and biological reactions for greater efficiency. They are ubiquitous in industrial processes, turning raw materials into useful products like milk to yogurt or petroleum into plastic jugs. In the human body, they are called enzymes, and help in creating signals for bodily functions and digesting food, among other tasks. Polymers have commonly been used in catalytic applications as supports for catalytic compounds because of their high surface area, porosity, surface functionality, and chemical inertness towards various harsh conditions. Recently a greater emphasis has been placed on using polymer materials themselves as catalysts, or in conjunction with other compounds to synergically enhance catalytic activity. These types of polymeric catalysts have been used in a range of fields including medical-based applications like antibacterial and wound healing, environmental remediation applications like pollutant degradation and sustainable synthesis, as well as energy applications like sustainable energy generation and storage. In this review, we discuss the various platforms developed for these three main fields and outline challenges and emerging research areas going forward.

1. Introduction

Catalysis is a key aspect in industrial and biological processes that allows for reactions to occur more quickly and efficiently [1]. This is achieved via the use of catalysts, which are substances that accelerate a chemical reaction without themselves being consumed in the process. They accomplish this by altering the reaction pathway, reducing the activation energy of the reaction, and selectively promoting specific reactions over others. The global catalyst market was valued at $USD 35.5 billion in 2020, and is expected to reach $USD 57.5 billion by 2030, with most of the market value share applied in petroleum refining, chemical synthesis, polymers and petrochemicals, and environmental uses [2]. The increase in demand for catalysts in these applications, amongst others, is driving the need for catalysts which allow for increased process optimization, yield, as well as reduced costs and energy consumption.

Catalysts can be broadly categorized into three main groups: homogenous, heterogenous, and biocatalysts (Fig. 1) [3]. For the former, the catalyst compound is in the same phase as the reactants, most commonly liquid phase, and can achieve high rates, with good selectivity. However, recovery of the catalytic element is complex and expensive [4]. Heterogenous catalysts are in a different phase than the reactants, making them readily separated and recycled, however generally at the cost of lower rates and selectivity [5]. Finally, biocatalysts involve natural proteins such as enzymes, which catalyze chemical reactions with high selectivity and efficiency, but tend to denature at harsh reaction conditions [6]. Although catalysts can be reused, they typically have reduced effectiveness due to fouling, poisoning, thermal degradation, leaching of active metal species, and/or other wear and tear effects [7]. Catalysts provide a transient weak bond with the reactant which compensates for the energy required to break the old bond until the new bond is formed to stabilize the product. The specific mechanism by which catalysts achieve this depends on the catalyst and reaction. As such, catalysts can also be categorized by mechanisms of action, such as acid-base, oxidation-reduction (redox), photo-, and coordination catalysis. Acid-base catalysis relies on molecules which can donate (acid) or accept (base) a proton (H^+) to increase the rate of the chemical reaction [8]. On the other hand, redox catalysis involves the transfer of electrons (e^-) between reactants in a chemical reaction [9]. In other words, the catalyst donates or accepts e^- to/from the reactants to facilitate the reaction. Photocatalysis also involves the transfer of electrons but instead relies on the absorption of light to

* Corresponding author.
E-mail address: rona.chandrawati@unsw.edu.au (R. Chandrawati).

https://doi.org/10.1016/j.apmt.2023.101937
Received 25 July 2023; Received in revised form 29 August 2023; Accepted 13 September 2023
Available online 18 September 2023
2352-9407/© 2023 The Author(s). Published by Elsevier Ltd. This is an open access article under the CC BY license (http://creativecommons.org/licenses/by/4.0/).

generate electron-hole pairs, usually via a semiconductor material [10]. Finally, in coordination catalysis, binding between the reactant and the catalyst takes place to improve the reaction rate [11].

Of the various types of catalysts available, polymeric materials have emerged as a type of catalyst, and are termed catalytic polymers. They can withstand harsh reaction conditions, are highly tuneable, can be heterogenous or homogenous, and can be less toxic due to the lack of metals. Polymers can act as catalysts by having certain functional groups incorporated within their chain to promote specific reactions. Additionally, they can provide a large surface area for reactant molecules to adsorb onto, and act as support materials for other catalytic substances [12], however these latter applications are outside the scope of this review.

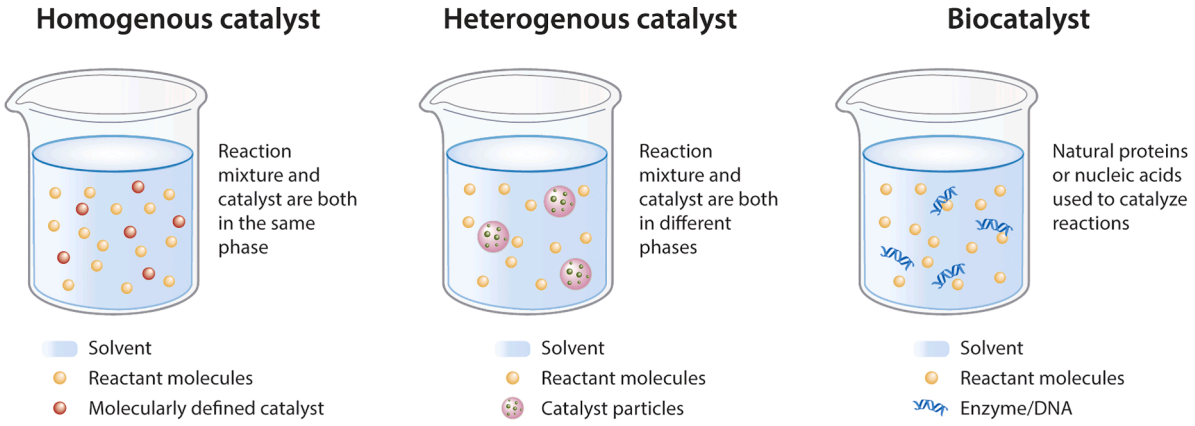
Herein, the use of polymeric materials as catalysts in the last 4 years in the field of medicine, environmental remediation, and energy generation will be evaluated. First, a brief overview of the most commonly used polymeric materials discussed within this review will be outlined. Then, the application of these catalytic polymeric materials in different fields will be evaluated. Specifically, cases where the polymers themselves act as a catalyst or synergistically perform catalysis in conjunction with other compounds will be discussed. Finally, an outlook on potential research avenues will be given.

2. Photocatalytic polymeric materials

Upon reviewing the literature, the aforementioned criterion narrowed down polymeric catalysts to those which primarily rely on the mechanism of action of photocatalysis. This means that some catalytic polymers like graphitic carbon nitride, covalent organic frameworks, and amine-rich polymers are consistently referenced within this review (Fig. 2). Consequently, a brief introduction of these most common polymeric materials will be included within the following section to familiarize the reader with each.

2.1. *Graphitic carbon nitride (g-C_3N_4)*

Graphitic carbon nitride (g-C_3N_4) is a synthetic polymer produced by the thermal polymerization of precursors such as cyanamide, dicyandiamide, and melamine. In contrast to the well-known metal-based photocatalyst, titanium dioxide (TiO_2) [13], g-C_3N_4 emerged as a promising metal-free, stable, and low-toxic alternative for photocatalysis. g-C_3N_4 has been widely investigated for the generation of



	Homogenous	Heterogenous	Biocatalyst
Advantages	All atoms act as active centres (i.e. high catalytic activity since reactants can quickly access catalyst) High selectivity Rare mass transfer limitations Can be rationally manipulated since chemical reactions are easy to characterize Easier to design	Easy to recover, regenerate and reuse Wide applications Low catalyst losses Durable Higher thermal stability	Allows for chemical reactions not feasible in aqueous media Can catalyze certain reactions in the reverse direction Good enantioselectivity Good substrate specificity Lack of side reaction of hydrolysis High efficiency of biocatalysts in water-organic mixtures
Disadvantages	Expensive/tedious to recover, regenerate and reuse Limited applications High catalyst losses Lower thermal stability	Low selectivity Severe mass transfer limitations Undefined structure/mechanism Only surface atoms act as active centres (i.e. when no more reactants can fit on the surface, reaction cycle cannot continue) Harder to design	Hard to recycle in non-covalently modified systems Labour and cost-intensive preparation Limited activity in most pure organic solvents Mass transfer limitations in the case of heterogeneous systems or viscous solvents Severely affected by harsh reaction conditions

Fig. 1. Catalyst classification. Catalysts can be divided into three main categories: (i) homogenous catalysts where the reaction mixture and catalyst are in the same phase, (ii) heterogenous catalysts where the reaction mixture and catalysts are in different phases, and (iii) biocatalysts where natural proteins or nucleic acids catalyze the reaction. The benefits and limitations of each are also outlined.

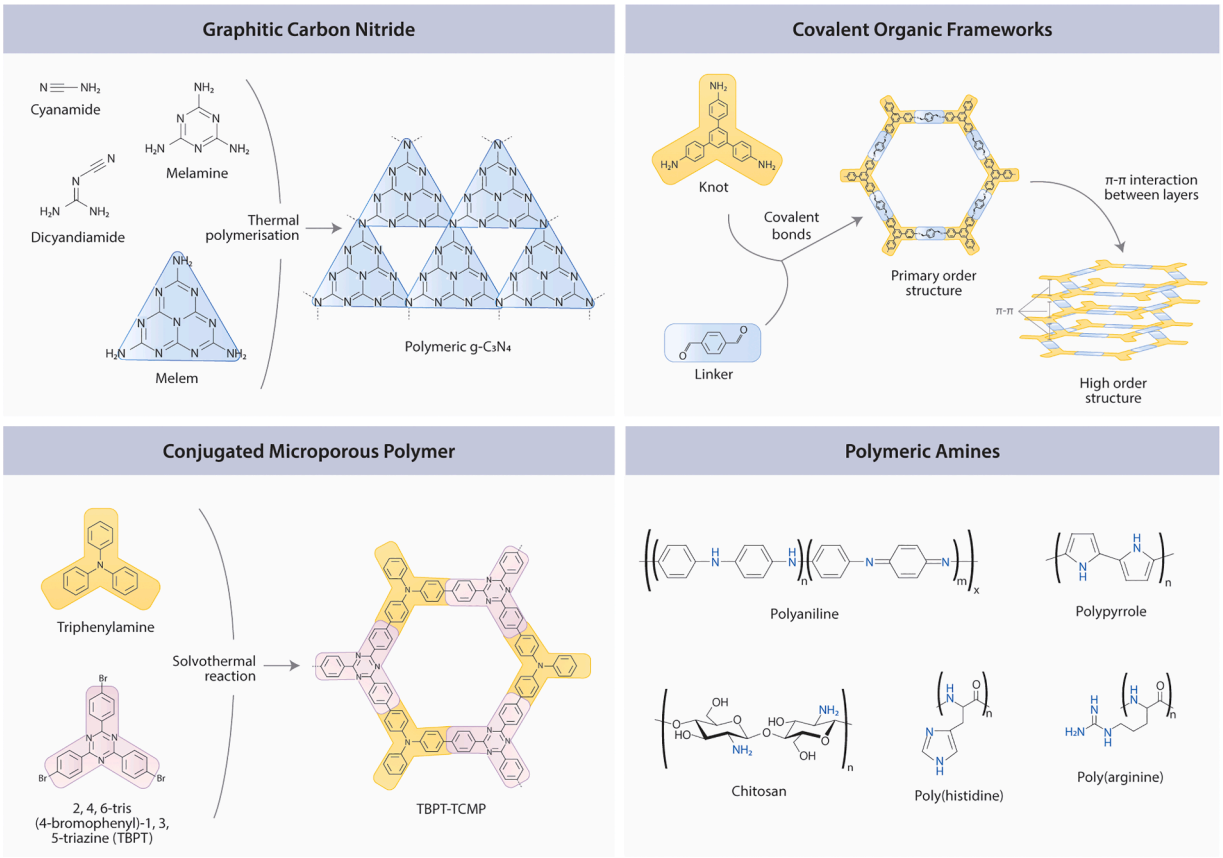


Fig. 2. Commonly researched photocatalytic polymers. Illustration of: (i) graphitic carbon nitride formation using different nitrogen containing precursor subunits, (ii) covalent organic framework formation using knots (organic molecules with various reactive points to enable branching of polymeric backbone) and linkers (organic molecules that connect knots), (iii) a triazine-based conjugated microporous polymer with a 3D network structure, and (iv) various natural (poly (histidine), poly(arginine), chitosan) and synthetic (polyaniline, polypyrrole) polymeric amines.

clean fuel (H_2) [14], carbon dioxide (CO_2) reduction [15], and the degradation of organic pollutants [16]. It is a type of semiconductor photocatalyst whose conduction (−1.4 eV) and valence (1.3 eV) band positions promote the harvesting of visible light towards oxidation and reduction processes, which is ideal for photocatalytic applications. For energy applications, the catalytic process generally consists of light harvesting, charge separation, and surface redox reactions on the photocatalyst. On the other hand, their main mechanism of action for pollutant degradation is via the light-triggered generation of reactive oxygen species (ROS) including hydroxyl radicals (·OH), superoxide anions (O_2^-), hydrogen peroxide (H_2O_2), and singlet oxygen (O_2), using water as an endogenous source. Bulk g-C_3N_4 is limited by a low specific surface area, high photoexcited electron and hole recombination rate, as well as restricted light absorption in the visible range [17]. As such, various strategies have been employed over the last decade to increase photocatalytic efficiency. These include: (i) morphological control which aims to provide more active sites, expand the visible-light response range, and shorten the carrier diffusion path [18], (ii) elemental doping with non-metal or metal atoms to generate intermediate band gaps and regulate the band structure of g-C_3N_4 [19], (iii) heterojunction construction to improve the separation and transport efficiency of electron-hole pairs [20], and (iv) nanomaterial composition to enhance charge transfer kinetics and electrical conductivity [21].

2.2. Covalent organic frameworks (COFs)

Covalent organic frameworks (COFs) are a class of covalently linked porous polymer networks with high crystallinity synthesized via condensation reactions [22]. They are widely employed in various fields including sensing [23], catalysis [24], energy storage [25], photo-energy conversion [26], and others [27], mainly due to their ordered structure, accessible surface area, porosity, thermal stability, and tunable functionalities [28]. As with g-C_3N_4, they employ similar mechanisms of action towards energy generation and pollutant degradation, i.e. light-triggered generation, migration, and separation of charge carriers for surface redox reactions and ROS generation, respectively [29]. They have effective light-harvesting capabilities due to π-conjugation and coherent band structures. Their light-harvesting capacity can be improved by modifying building blocks, the structure and interlayer interactions, as well as transmission distance, bestowing a highly controllable design for photocatalytic applications [30]. COFs are generally limited by their poor electrical conductivity and low stability in aqueous/organic conditions. As such, research has been conducted to improve their performance via the addition of functional groups [31], by increasing their surface area and pore size [32], adjusting molecular design [33], as well as the addition of active sites [34].

2.3. Conjugated microporous polymers (CMPs)

Conjugated microporous polymers (CMPs) are the amorphous analogues of COFs [35]. CMPs are a 3D semiconducting polymer with rigid aromatic groups linked together, forming π-conjugated microporous networks [36]. The increase in research surrounding CMPs arises from the variety of building blocks available, which allows for specific functionalities and structures [37]. The alternation between single and double-/triple-bonds within the network gives CMPs unique electronic properties, and have therefore been used in a range of areas including gas separation [38], chemical encapsulation [39], catalysis [40], sensing

[41], as well as energy storage [42].

2.4. Polymeric amine

Polymeric amine refers to a class of polymers which contain a high concentration of primary (R-NH_2), secondary (RR'-NH), and/or tertiary (RR'R''-N) amine groups in their backbone and/or side branches. These include natural polymers like chitosan, polydopamine (PDA), and poly (amino acids), as well as synthetic polymers including polyaniline (PANI), polypyrrole (PPy), and polyethyleneimine (PEI) [43]. In most cases, the amine groups act as an absorption site to increase the pollutant concentration near a photocatalyst's microenvironment. This is achieved via their cationic [44] and anion-exchange [45] behavior, coordination/complexation sites [46], and hydrogen bonding [47], among others [48,49]. In terms of inherent catalytic activity, not many polymeric amine possess it, however, they are usually used in conjunction with other materials in photocatalytic applications. The nitrogen of the amino groups have been shown to contribute to heterojunctions which promote charge separation and shift the photo-response towards the visible range [50]. In other words, the introduction of these polymeric amine results in significantly enhanced visible-light driven photocatalytic activity due to improved separation of photoexcited charge carriers, wider light absorption range, and increased reactant adsorption [51]. The mechanism of action involves the generation of radicals which target organic pollutants via oxidative degradation reactions [52].

3. Polymeric materials as catalysts in various fields

Regardless of the field, i.e. medical, environmental, or energy, the mechanism of action for polymeric material to act as catalysts are similar. It often involves light harvesting to photocatalytically generate heat, reactive oxygen species (ROS), and/or surface redox reactions (Fig. 3). The following section will outline the use of these catalysts in more detail.

3.1. Medical-based applications

The use of metal catalysts for physiological applications is challenging as they can be a source of toxicity due to leaching, even when immobilized [53]. Zeolite catalysts, though generally considered biocompatible, are not naturally found in the body, and may stimulate the immune system by promoting an inflammatory response [54]. The use of polymeric materials as catalysts circumvents this as they are organic molecules that are biocompatible and biodegradable. The following section will discuss various medical-based applications where polymers have been used for a catalytic process.

3.1.1. Antibacterial

With the increasing reliance on antibiotics in recent years, the resistance of bacteria towards them has almost tripled in the last two decades [55]. As such, alternative strategies for effective sterilization have been considered. Traditional methods include chlorination and UV irradiation [56,57], however photocatalysis has emerged as a preferred choice whereby the bactericidal effect arises from the catalytic generation of ROS or heat [58]. A highly investigated polymeric material in this regard involves g-C_3N_4. Despite their antibacterial properties without the addition of additives [59], several strategies have been employed to further increase their performance. Most commonly, these include the addition of nanoparticles [60], silver-based substances [61], doping [62], different morphologies [63] and heterostructures [64], as well as the addition of amine-rich polymers like PEI [65] and PANI [66]. These approaches have proven effective against *Pseudomonas putida, Staphylococcus aureus*, and/or *Escherichia coli*, achieving high sterilization rates of >80% within 0.3–2 h. In fact, some studies have reported bactericidal properties towards chloramphenicol-resistant *E. coli* and methicillin-resistant *S. aureus* (MRSA) of 100% within 30 min (Fig. 4ai-ii) [67]. This was achieved by the synergy between photocatalysis and nanozyme catalytic activity. For the former, doping g-C_3N_4 with sulfur (g-SCN) leads to a broadening of the absorption spectrum which promotes photocarrier separation, thus increased photocatalytic

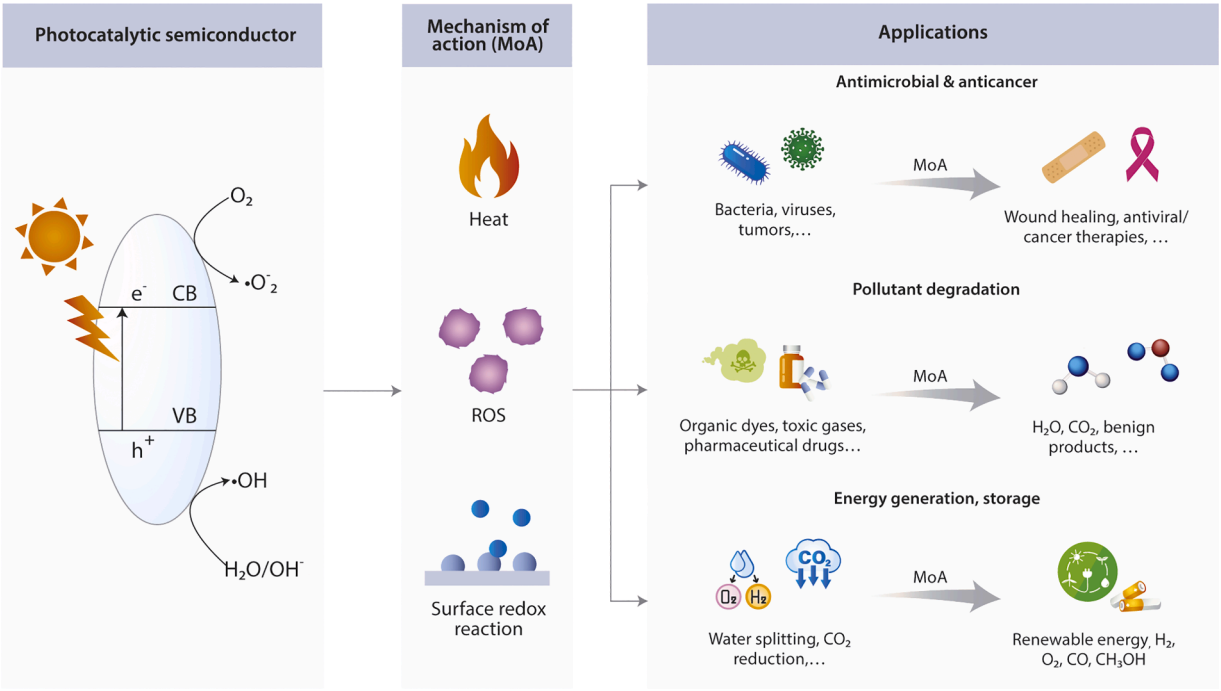


Fig. 3. Mechanism of actions of polymer catalysts for various applications. The use of polymer catalysts in medical-, environmental-, or energy-based applications involves the use of light to trigger the photocatalytic generation of heat, ROS, and/or redox surface reactions. In most cases, medical-based applications such as antimicrobial applications rely on heat and/or ROS generation, environmental-based applications such as pollutant degradation rely on ROS generation, while energy-based applications such as energy generation rely on surface redox reactions.

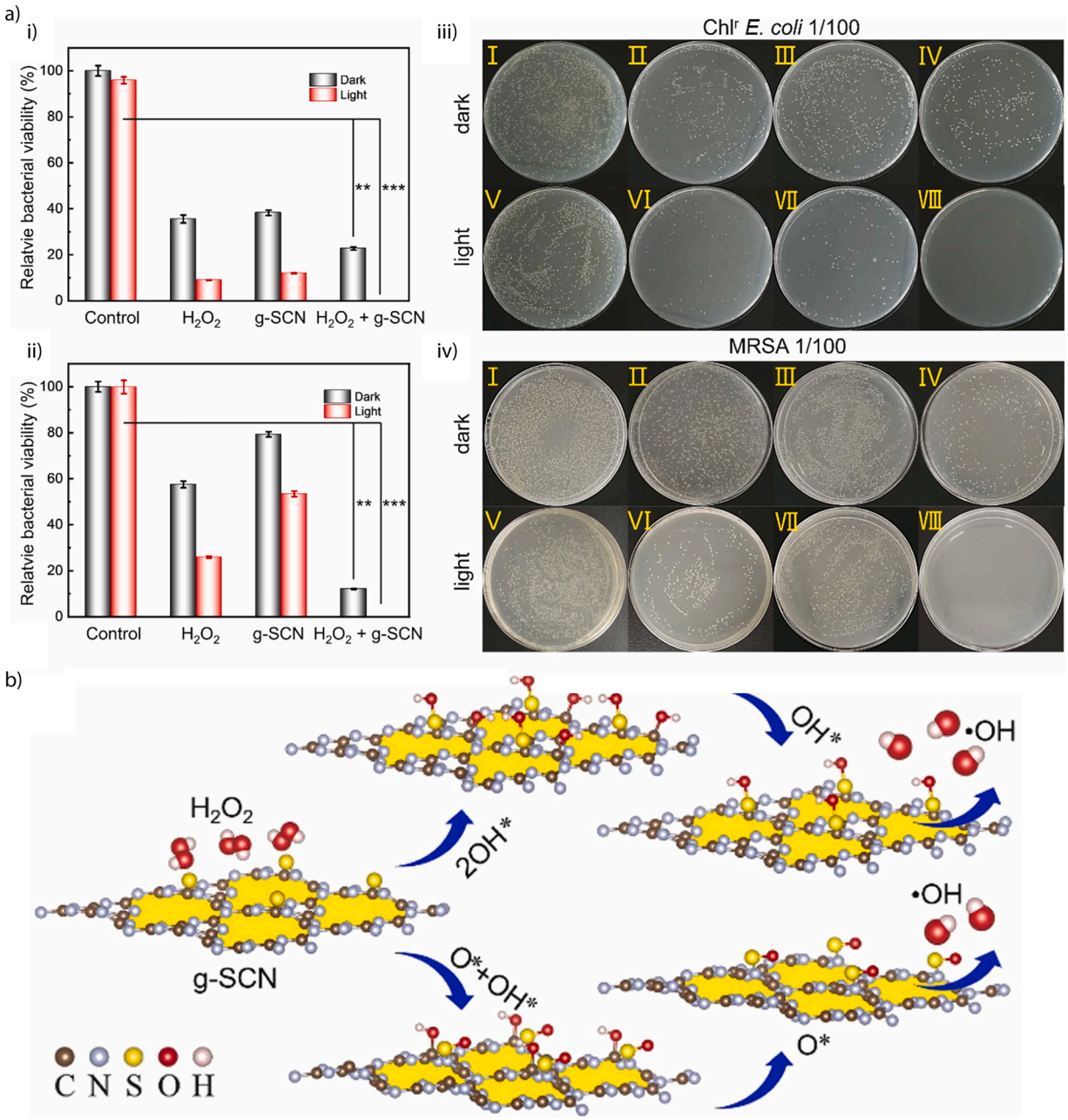


Fig. 4. Catalytic polymeric materials (g-C_3N_4) for antibacterial applications. a) Relative survival rate of (i) chloramphenicol-resistant *Escherichia coli* and (ii) methicillin-resistant *Staphylococcus aureus* under different conditions with and without light. Photographs of bacterial colonies for (iii) chloramphenicol-resistant *Escherichia coli* and (iv) methicillin-resistant *Staphylococcus aureus*. (I) Control, (II) H_2O_2, (III) g-SCN, (IV) g-SCN + H_2O_2, (V) control + light, (VI) H_2O_2 + light, (VII) g-SCN + light, and (VIII) g-SCN + H_2O_2 + light. b) Schematic illustration of generation of ·OH during H_2O_2 decomposition using g-SCN. Reprinted with permission from [67]. Copyright 2023, Elsevier.

performance. For the latter, the sulfur element coordinates with nitrogen in g-C_3N_4, endowing them with peroxidase-like catalytic activity. Collectively, this led to a greater generation of ·OH radicals which have high bactericidal properties (Fig. 4b). This was also visually observed from the bacterial culture, where no growth of bacterial colonies were observed when using g-SCN + H_2O_2 + light (Fig. 4aiii-iv). Furthermore, the increased specific surface area of g-SCN also contributed to more effective trapping of bacteria. Similar doped formats, like phosphorus doping [68], have also achieved high rates of sterilization.

Antibacterial attempts employing COFs have also been developed relying on various bactericidal mechanisms including photocatalytic sterilization [69], cationic sterilization [70], and biomolecular composites [71]. Photocatalytic antibacterial platforms are also one of the most popular approaches, where the generation of ROS for bacteria inactivation is improved by the inclusion of porphyrins [72], triazine [73], 2D layered transition metal carbides or carbonitrides [74], as well as non-metals [75]. The antibacterial effect for all these platforms towards *Pseudomonas aeruginosa, Enterococcus faecalis, S. aureus*, and/or *E. coli* was observed upon irradiation with white light, achieving sterilization efficiencies of >90% within 1–4 h. Recent studies have even involved synergistic bacterial inhibition by integrating photodynamic, photothermal, and peroxidase-like enzymatic activities [76]. To achieve this, a covalent organic framework (TAPP-BDP) with a unique donor-acceptor structure was synthesized consisting of a narrow energy gap and extended π-conjugated skeleton for improved ROS generation and enhanced absorption in the near infrared (NIR), respectively

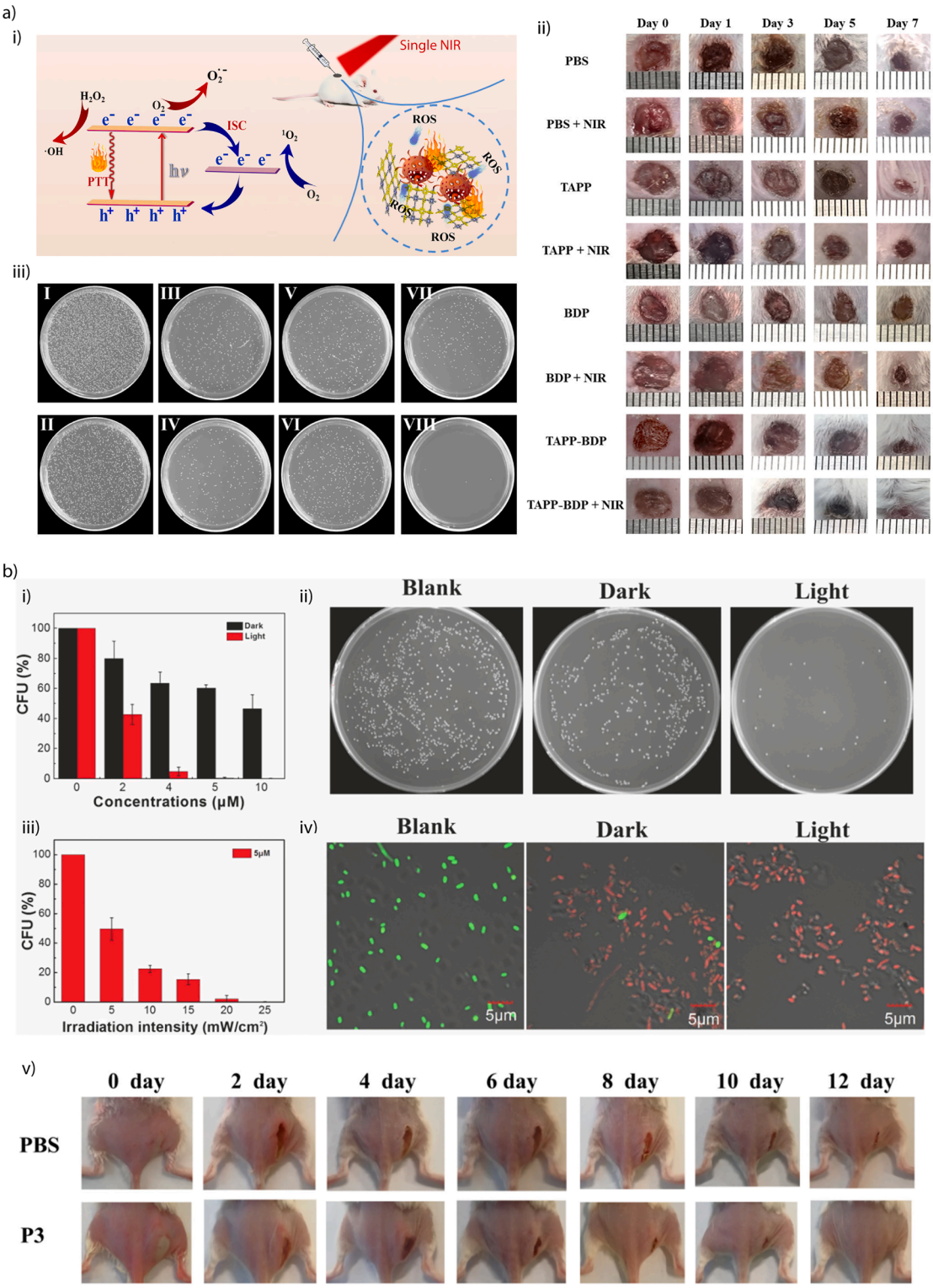


Fig. 5. Catalytic polymeric materials for antibacterial applications. a) (i) Illustration of triple synergistic antibacterial effect of TAPP-BDP under irradiation with a single NIR light. (ii) Wound healing images of mice under different conditions. (iii) Photographs of bacterial colonies from the homogenized tissue dispersions of the infection sites of mice for each condition. (I) PBS, (II) PBS + NIR, (III) TAPP, (IV) TAPP + NIR, (V) BDP, (VI) BDP + NIR, (VII) TAPP-BDP, and (VIII) TAPP-BDP + NIR. Reprinted with permission from [76]. Copyright 2022, American Chemical Society. b) (i) Antibacterial activity of red fluorescence polymers toward ampicillin-resistant *Escherichia coli* TOP10 with and without irradiation of white light. (ii) Photographs of bacterial colonies of ampicillin-resistant *Escherichia coli* TOP10 treated with red fluorescence polymers with and without irradiation of white light. (iii) Antibacterial activity of red fluorescence polymers toward ampicillin-resistant *Escherichia coli* TOP10 under different intensities of light irradiation. (iv) Confocal laser scanning microscopy images of ampicillin-resistant *Escherichia coli* TOP10 stained by PI (propidium iodide) and SYTO9 after treating with red fluorescence polymers with and without irradiation of white light. v) Photographs of mice infected with *Staphylococcus aureus* within 12 days postinjection under treatment of PBS or the red fluorescent polymer. Reprinted with permission from [77]. Copyright 2018, American Chemical Society.

(Fig. 5ai). The antibacterial properties of TAPP-BDP was demonstrated *in vivo*, by evaluating wound healing conditions at different time intervals in mice (Fig. 5aii). After a 5-day treatment, redness and swelling was reduced for the NIR exposed TAPP-BDP treatment, with both the wound area and infection degree being lower. On the 7th day, infection recovery and wound healing was superior compared to other treatments. Furthermore, wound skin tissues were harvested and minimal number of bacterial colonies were observed for the TAPP-BDP/NIR group (Fig. 5aiii). Alternatively, red fluorescence polymers bearing quaternary ammonium groups can also be developed for bactericidal applications [77]. These polymers have shown to be effective towards Gram positive and negative bacteria as well as fungi, with 100% bactericidal effect towards ampicillin-resistant *E. coli* TOP10 (Fig. 5bi-ii). The antimicrobe activity arises from "light" and "dark" toxicity. For the former, the

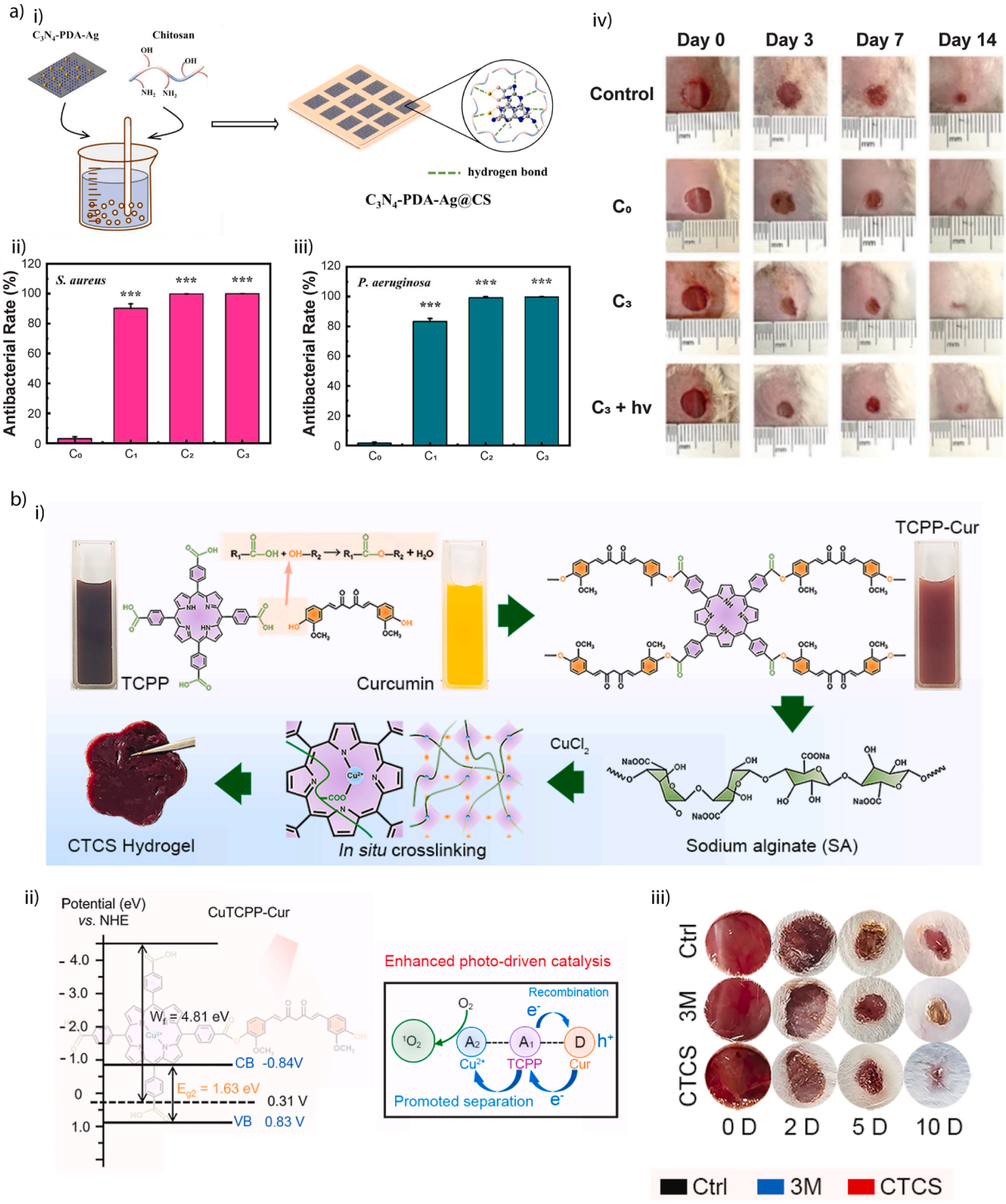


Fig. 6. Catalytic polymeric materials for wound healing applications. a) (i) Illustration of synthesis of chitosan-based C_3N_4-PDA-Ag composite dressing (C_3N_4-PDA-Ag@CS). Antimicrobial rate towards (ii) *Staphylococcus aureus* and (iii) *Pseudomonas aeruginosa* after 10 min of irradiation. (iv) Wound healing photographs of the control, C0, C3, and C3 + hv groups. Reprinted with permission from [86]. Copyright 2023, Elsevier. b) (i) Schematic diagram of CTCS hydrogel synthesis. (ii) Schematic diagram of the photocatalysis mechanism of CuTCPP-Cur nanoparticle. (iii) Wound healing photographs for the control, 3M wound dressing, and CTCS hydrogel groups after 0, 2, 5, and 10 days. Reprinted with permission from [88]. Copyright 2023, Elsevier.

backbone structure of the polymer consists of fluorene, benzene, thiophene, and benzothiadiazole units, which can produce ROS upon light irradiation (Fig. 5biii-iv). The "dark" toxicity arises from the quaternary ammonium groups in the side chains, which sensitize oxygen molecules to generate ROS. Moreover, their applicability for wound healing and disinfection *in vivo* without causing damage to tissue was demonstrated, providing efficient antimicrobial and clinical pathogenic treatment (Fig. 5bv).

3.1.2. Wound healing

There are two main reasons for delayed wound healing: (i) excessive inflammatory response and/or (ii) bacterial presence which make the environment unsuitable for cell proliferation [78]. As bacteria inhibition is key, the previously described antibacterial properties of catalytic polymeric materials are closely linked with enhanced wound healing. A recently investigated approach involves light-to-heat conversion from polydopamine (PDA). PDA has NIR response photothermal catalytic characteristics which provide antibacterial properties, i.e. the high temperatures generated by NIR accelerate cell death. This has been demonstrated with high sterilization efficiencies (>95%) for *E. coli* [79], *S. aureus* [80], and methicillin-resistant *S. aureus* [81]. It should be noted that for these cases, PDA is usually complexed with bactericidal substances, whereby the synergy between both leads to an enhanced antibacterial effect. Nevertheless, studies have also been shown to achieve high sterilization rates (>96% within 10 min) towards *E. coli* and *S. aureus* when employing only PDA nanoparticles within food gum matrices [82]. In this approach the role of PDA is twofold. Firstly, it interacts with the food gum matrix to form a hydrogel with excellent mechanical strength and high elasticity, enabling it to adapt to the wound shape. Secondly, it acts as a photothermal transduction agent to convert NIR laser radiation to heat, triggering bacterial death. This hydrogel demonstrated accelerated wound healing *in vivo* by reducing the inflammatory response and promoting vascular reconstruction. As expected, g-C_3N_4 has also been extensively investigated for wound healing applications [83], with various examples described within the previous section, and have shown highly efficient (>99% within 10–15 min) sterilization of bacteria with successful *in vivo* wound healing [84, 85]. In a recent approach, a carbon nitride-PDA-silver (C_3N_4-PDA-Ag) complex compounded with chitosan (CS) was developed to achieve a highly effective antimicrobial effect (C_3N_4-PDA-Ag@CS; Fig. 6ai) [86]. In this design, PDA has two functions: (i) it enhances the photocatalytic activity of C_3N_4 through π-π* interactions and (ii) it reduces Ag^+ to AgNPs. Thus, a synergistic antibacterial effect was achieved with the enhanced photocatalyst and the metal nanoparticles. To assess the antibacterial activity towards *S. aureus* and *Pseudomonas aeruginosa*, the OD measurement of the bacterial solution was used. It was observed that the OD did not differ significantly between the control and CS only (C0). However, as the concentration of the C_3N_4-PDA-Ag complex increased (C1, C2, C3), the absorbance value decreased, suggesting high antibacterial activity. The optimised complex (C_3N_4-PDA-Ag@CS) was assessed against *S. aureus* and *Pseudomonas aeruginosa* and showed high inhibition (>80%) within 10 min (Fig. 6aii-iii). More importantly, it also promoted wound healing in infected mice by facilitating collagen deposition and accelerating epidermal regeneration (Fig. 6aiv). As with g-C_3N_4, COFs have also been extensively applied for wound healing applications [87]. For instance, curcumin (Cur) can be linked to tetra-(4-carboxyphenyl) porphyrins (TCPP) and then combined with sodium alginate (SA) and Cu^{2+} to form a hydrogel with photocatalytic and anti-inflammatory properties (CTCS; Fig. 6bi) [88]. The mechanism behind it involves the electron-rich Cur and the photosensitizer TCPP forming a π-conjugated donor-acceptor COF-like structure. Under irradiation, electrons easily transfer from the Cur to the TCPP, inhibiting the complexation of the photogenerated electron-hole pair. Introducing Cu^{2+} reduces the band gap and promotes charge separation, thus improving the photocatalytic effect (Fig. 6bii). The hydrogel can achieve high sterilization rates (>98% within 20 min) against *S. aureus* and *E. coli* and has shown *in vivo* wound healing and tissue regeneration via the change in expression of inflammatory factors (Fig. 6biii). It is also possible to load COFs with drugs which compound the antibacterial benefits [89]. Recently, a biodegradable porphyrin-based COF nanosheet was synthesized which synergized photodynamic and photothermal therapy under red light irradiation [90]. The red light also triggered the release of nitric oxide (NO; a known antibacterial agent) for gaseous therapy. The developed platform could efficiently generate ROS and high temperatures, release NO under laser irradiation, exhibit antibacterial properties against *E. coli* and *S. aureus*, inhibit inflammatory cytokines, and promote wound healing in mice, all while being biodegradable and biocompatible.

3.1.3. Antiviral

The tuneable chemical structure and composition of polymers compounded with their high molecular weight and buffering effect, endow them with unique antiviral capabilities. Most commonly, they have been used for this application as drug carriers [91], lipid-membrane disrupting agents [92], coatings [93], and ion-releasing platforms [94], among others [95–97]. The antiviral effect for these systems is carried out via two different approaches. The polymer is used as a stabilizing matrix which protects and delivers an antiviral agent, or the polymer itself is used as the antiviral agent which binds to the virus surface and inhibits infection. Polymers can also be used for antiviral catalytic applications; however, these are not as common. This is likely due to the inactivation behavior of ROS which have been shown to be microorganism-dependent [98]. As with bacteria, the inactivation mechanism can proceed via three main routes: (i) physical damage to the virus, (ii) photocatalytic release of metal ions inducing metal ion toxicity, and (iii) chemical oxidation via ROS to degrade the cell wall [99]. Chemical oxidation is the most widely used approach due to its high efficiency. With the advent of COVID-19, face masks have become the recommended prophylactic measure to contain the virus transmission, with several reports attempting to improve upon their intended use by increasing their re-usability [100], providing therapeutic benefit [101], and of relevance to this review, adding polymeric-based antiviral coatings [102]. For instance, COFs loaded with silver nanoparticles (AgNPs) can be deposited onto the outer layer of non-woven PET fabric face masks endowing them with solar-powered antibacterial and antiviral properties [103]. This is achieved via photothermal (PTT) and photodynamic therapy (PDT), which can induce hyperthermia and generate ROS under light irradiation, respectively, leading to microbial damage. Moreover, AgNPs are known to act against bacteria, viruses, and fungi by interacting with their cell membranes, whilst enhancing PTT and PDT due to their inherent plasmonic nature. Virucidal performance was also observed with various metal-free photocatalytic-based graphitic carbon nitride platforms [104]. By oxygen doping g-C_3N_4 and integrating it with hydrothermal carbonation carbon, human adenovirus type 2 can be inactivated [105]. This is due to the strong visible light absorption and narrow band gap of the complex, which enhances charge separation and enables the production of ROS as strong antiviral agents. As such, complete antiviral effects within 2 h in drinking water can be achieved. Other similar efficient strategies relying on ROS generation have also been reported with rapid (<2 h) and effective virucidal capabilities [106].

3.1.4. Cancer therapy

Cancer is one of the leading causes of death worldwide and various strategies have been devised to tackle this issue, the most common of which include chemotherapy, surgery, and radiotherapy [107]. Advances in the STEM fields have led to the development of alternative approaches, including PDT and PTT. The former relies on the generation of ROS to cause oxidative damage to cellular components while the latter involves heat generation to ablate the tumor. Semiconductor-based polymers such as COFs are ideal candidates for these emerging strategies. Although commonly used for chemotherapy

drug delivery applications via pH- [108], redox- [109], and GSH-responsive platforms [110], reports have also shown the polymers themselves exhibiting tumor inhibiting capabilities via PDT [111,112] or PTT [113,114] strategies. Moreover, some of these photocatalytic approaches have shown efficient anticancer properties whilst allowing for imaging applications [115,116]. For instance, a dye-labelled oligonucleotide can be integrated onto porphyrin-based COF nanoparticles (COF-survivin) for effective cancer diagnosis and therapy [117]. In this case, the dye is quenched by the COF due to FRET (fluorescence resonance energy transfer), but in the presence of the cancer biomarker survivin mRNA, the fluorescence signal is recovered (Fig. 7ai). Upon irradiation with NIR light, enhanced ROS generation is observed due to the crystalline reticular structure of the COF. The performance of this platform was demonstrated *in vivo*, allowing for selective cancer imaging and elimination of the malignant tumor (Fig. 7aii-iii). In essence, these polymeric catalysts allow for the integration of diagnosis and treatment. In fact, this "dual-purpose" approach also inspired other synergistic antitumour strategies. By combining different therapies, such as chemotherapy with PDT/PTT [118,119] or PDT with PTT [120,121], an enhanced therapeutic effect can be achieved. For instance, a non-porphyrin containing COF nanoparticle can be developed with inherent PDT capabilities and be further conjugated with CuSe, a photothermal agent, to form a dual functional COF with synergistic phototherapeutic effects *in vivo* (Fig. 7bi) [122]. This platform shows enhanced therapeutic effect in killing cancer cells and inhibiting tumor growth compared to its pristine counterpart (Fig. 7bii). Unexpectedly, g-C_3N_4 has not been as thoroughly investigated compared to COFs for anticancer applications [123], with most studies focusing on g-C_3N_4 in the form of NPs [124], QDs [125], or nanosheets [126] for PDT and PTT applications. The addition of elements such as AuNPs [127] or metal cations [128] have also been investigated to enhance their therapeutic benefit. As with COFs, the development of multifunctional nanoplatforms is becoming more common [129]. For instance, ultrathin graphitic carbon nitride nanosheets loaded with a hypoxia-targeting platinum(IV) prodrug can be developed which generate ROS in addition to DNA binding platinum species to enhance antiproliferation of regulatory transcription factors [130]. Even further, g-C_3N_4 QDs can be used for imaging and chemo-photodynamic combination therapy [131]. This is achieved by first introducing carboxyamino-terminated oligomeric polyethylene glycol and folic acid onto the surface of the g-C_3N_4 QDs, endowing them with physiological stability, blue fluorescence, biocompatibility, and ROS generating capabilities. Non-covalently loaded doxorubicin enables its chemotherapy function. Compared with free doxorubicin, g-C_3N_4 QDs demonstrate more efficient chemotherapy to HeLa cells. This is due to improved folate receptor-mediated cellular uptake and intracellular pH-triggered drug release. In addition, the complex shows enhanced inhibition of cancer cell growth compared to sole chemotherapy or PDT.

3.2. Environmental-based applications

The increase in standard of living, population, and industrialization, has led to significant environmental pollution, with severe negative impacts on human health, wildlife, and natural resources. These effects are compounded if the pollutants accumulate in the environment, potentially leading to permanent damages. Most of these pollutants are anthropogenic, including toxic organic dyes, agricultural and pharmaceutical wastage, heavy metals, as well as toxic gasses (CO, SOx, NOx) [132–137]. With the current demand for energy efficient systems, a shift has occurred towards the development of techniques that can degrade

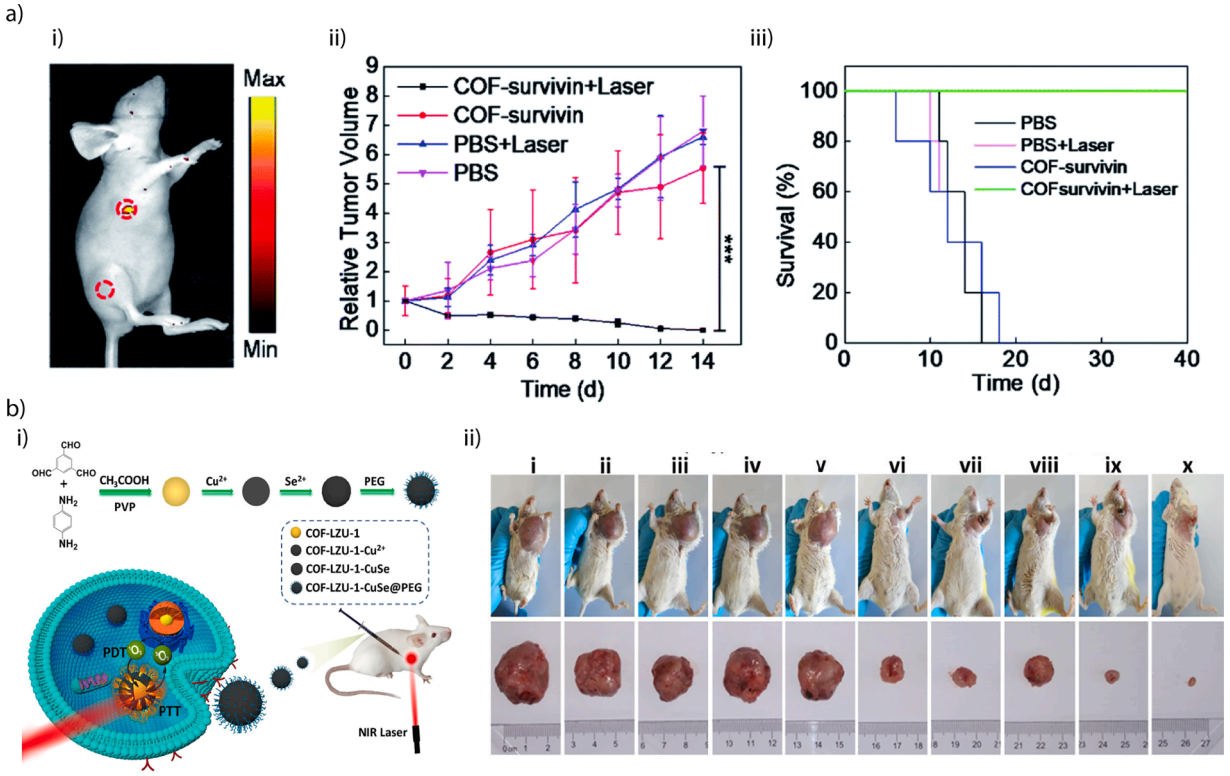


Fig. 7. Catalytic polymeric materials for cancer therapy applications. a) (i) *In vivo* fluorescence imaging of tumor-bearing nude mice after injected with COF-survivin. (ii) Relative tumor volume after different treatments (PBS, PBS+laser, COF-survivin, COF-survivin+laser). (iii) Survival curves of tumor-bearing mice after different treatments (PBS, PBS+laser, COF-survivin, COF-survivin+laser). Reprinted with permission from [117]. Copyright 2020, Royal Society of Chemistry. b) (i) Schematic illustration of the synthesis of COF–CuSe nanoparticles for combined PTT and PDT. (ii) Photographs of tumor-bearing mice and (ii) tumors dissected from mice. I: control; ii: PDT; iii: PTT; iv: COF; v: COF–CuSe; vi: COF + PDT; vii: COF + PTT; viii: COF–CuSe + PDT; ix: COF–CuSe + PTT; x: COF–CuSe + PDT + PTT. Reprinted with permission from [122]. Copyright 2019, American Chemical Society.

these compounds while consuming little energy. Polymeric catalysts have been used in this regard for a range of different pollutants including flame retardants [138], plasticizers (BPA) [139], sulfur-rich compounds [140], polymers found in oilfield sewage [141], hydroxyl-containing pollutants [142], and nitrobenzene [143]. However, the most researched pollutants involve organic dyes, pharmaceutical drugs, and toxic gasses. As such, the following section will focus on strategies employed to degrade these latter contaminants.

3.2.1. Organic dye degradation

The annual worldwide production of synthetic dyes is estimated at 70 million tonnes and is a major contributing factor towards water contamination [144]. These dyes are categorized based on their structure and application, ranging from cosmetics, leather, wool, and silk, to medicine, ink, and paper. Regardless of their category, they can act as ecotoxicological threats with negative effects on living organisms [145]. This is because these toxic chemicals that are discharged as effluent into wastewater remain in water and soil over extended periods of time, resulting in reduced soil fertility and photosynthetic activity of plants as well as increased biochemical and chemical oxygen demand. Moreover, they can enter the food chain, leading to bioaccumulation and thus promoting toxicity, mutagenicity, and carcinogenicity [146]. Traditional purification systems like flocculation or electrochemical treatment produce harmful by-products which contribute to secondary pollution [147] or high energy consumption [148], respectively. As such, catalytic polymeric materials have been considered as attractive alternatives for this application, specifically the advanced oxidation technology: photocatalysis. Three techniques are commonly used, among others, to evaluate the performance of these systems including: (a) the photocurrent density, (b) the Nyquist plot, and (c) the catalytic activity (Fig. 8). The former refers to the rate of flow of electrical current produced by the photoexcited charge carriers under visible light illumination. A higher photocurrent density indicates better light absorption, efficient charge separation, and enhanced photoelectrochemical activity. In other words, the catalyst's ability to convert light energy into useful chemical reactions, such as water splitting or pollutant degradation (Fig. 8a). The Nyquist plot, also known as electrochemical impedance spectroscopy (EIS), provides information about charge transfer resistance, surface recombination rates, and other kinetic processes occurring at the electrode-electrolyte interface. A well-defined Nyquist plot with a semicircular arc indicates efficient charge transfer, while deviations from this behavior might suggest limitations in charge separation and transfer efficiency. In addition, a smaller arc radii implies a higher electron transfer efficiency and a smaller interfacial resistance (Fig. 8b). Finally, the catalytic activity of the polymer is evaluated by measuring the decomposition rate by monitoring the change in the contaminant concentration over time under visible light irradiation (Fig. 8c).

Graphitic carbon nitride has been applied for the degradation of various organic dye pollutants, most commonly methylene blue [149], methylene orange [150], and rhodamine B [151]. In all cases, the degradation mechanism is the same, whereby ROS are photo-catalytically generated to degrade the pollutant. Instead, the variable that researchers investigate is the ability to enhance the degradation efficiency by modifying g-C_3N_4 via the addition of nanoparticles [152], polymers like polydopamine (PDA) [153], doping [154], as well as morphological changes [155]. For instance, highly condensed few-layered nanosheets of g-C_3N_4 (CM-CN) can be developed by mixing cyanuric acid and melamine in water and calcinating the mixture. The nanosheet structure leads to a higher charge mobility due to the reduced charge diffusion length within the smaller and thinner nanosheets compared to pristine g-C_3N_4 (M-CN; Fig. 9ai). Furthermore, the reduced arc diameter of the Nyquist plot for the nanosheet structure depicts a decrease in charge transfer at the catalyst interface when the charge carriers transfer from the surface to the electrolyte (Fig. 9aii). These photoelectrochemical characteristics compounded with the high surface area and pore volume, lead to complete degradation of rhodamine B within 15 min, even after five successive runs, as well as tetracycline within 90 min (Fig. 9aiii-iv) [156]. Alternatively, a g-C_3N_4/TiO_2 nanocomposite can be synthesized which show enhanced catalytic degradation towards methylene blue compared to its pure counterparts, i.e. TiO_2 or g-C_3N_4. However, the addition of boron nanoparticles further improves this degradation. This is attributed to the electron transfer from the composite to the elemental boron due to the heterojunction between them, achieving efficiencies of >80% within 3 h [157].

Similarly, COF-based platforms also rely on ROS generation for the degradation of dye pollutants including methylene blue [158], methylene orange [159], rhodamine B [160], orange II [161], and various nitroaromatic compounds [162], among others [163,164]. Recently, imine-linked COFs have been shown to exhibit efficient photodegradation of azo dyes, whereby the $N = N$ bonds are broken by superoxide radicals within 1.5 h [165]. Moreover, the catalyst can be recovered from the dye solution and used at least three times with minimal loss in activity. This performance is attributed to their densely conjugated structure, large absorbance range, excellent dispersibility in water, and high surface area, which allows for ROS generation towards dye degradation. The catalytic degradation was demonstrated for mordant black 3, mordant black 17, mordant red 7, eriochrome black A, and eriochrome black T, with efficiencies ranging from 40 to 90% depending on the dye. Of greater interest is the ability of these polymeric catalysts to perform multiple functions, i.e. degrade different types of pollutants at the same time [166,167]. An example involves a AgI modified COF (COF-PD/AgI) which was fabricated to photocatalytically degrade bacteria, organic pollutants, as well as antipyretic drugs, specifically *E. coli*, rhodamine B, and acetaminophen, respectively [168]. For the former, a negligible decrease in viable *E. coli* was observed when exposed to either COF-PD or a physical mixture of COF-PD and AgI with

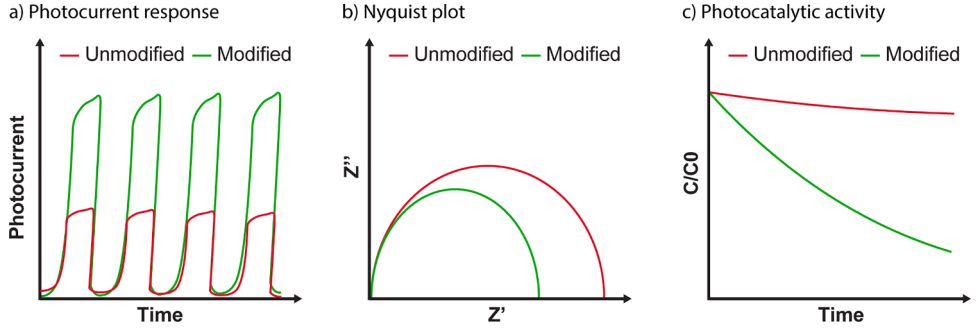


Fig. 8. Performance indicators for polymeric catalysts in pollutant degradation. Representative (a) transient photocurrent response, (b) electrochemical impedance spectroscopy plot (Nyquist plot), and (c) photodegradation kinetics of an unmodified polymeric catalyst (e.g. pristine g-C_3N_4) and a modified one (e.g. g-C_3N_4 nanosheets).

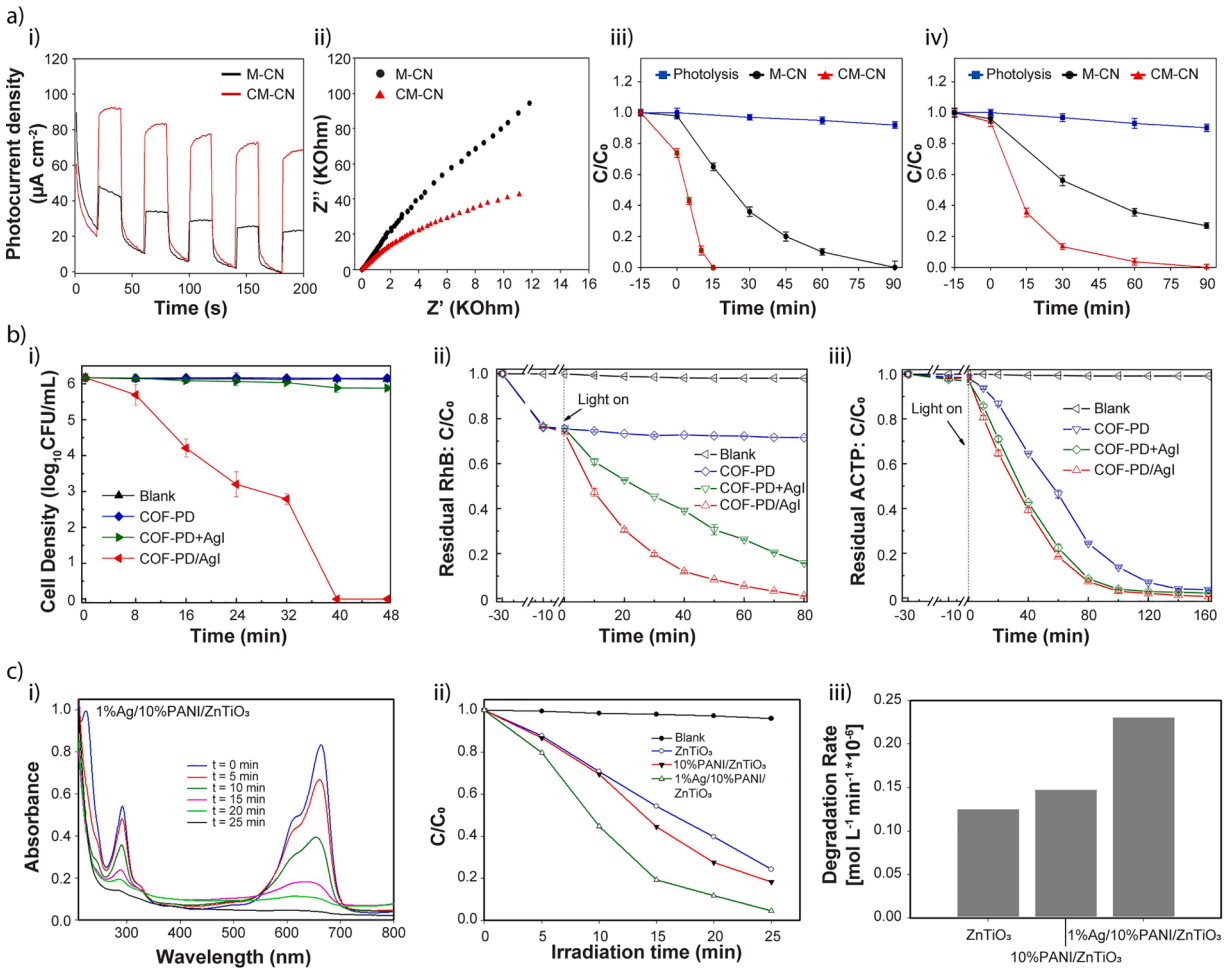


Fig. 9. Catalytic polymeric materials for organic dye degradation. a) (i) Transient photocurrent response and (ii) electrochemical impedance spectroscopy plot of pristine g-C_3N_4 (M-CN) and graphitic carbon nitride nanosheets (CM-CN). Photolysis and photodegradation kinetics for (iii) rhodamine B and (iv) tetracycline. Reprinted with permission from [156]. Copyright 2020, American Chemical Society. b) Photocatalytic performance of AgI modified COF towards (i) *Escherichia coli* disinfection, (ii) rhodamine B degradation, and (iii) acetaminophen degradation. Reprinted with permission from [168]. Copyright 2020, Elsevier. c) (i) Absorption spectra, (ii) change in concentration vs. irradiation time, and (iii) comparison of degradation rate of different nanocomposite photocatalysts ($ZnTiO_3$, 10%PANI/$ZnTiO_3$, and 1%Ag/10%PANI/$ZnTiO_3$) for the degradation of methylene blue. Reprinted with permission from [185]. Copyright 2021, Elsevier.

visible light irradiation (Fig. 9bi). On the other hand, complete disinfection was achieved by COF-PD/AgI within 40 min with visible light irradiation, indicating a greatly enhanced bactericidal effect. It should be noted that due to the small amount of silver ions released from COF-PD/AgI, they cannot be considered the main contributor to the photocatalytic disinfection [169]. Instead, the reactive species ($\cdot O_2^-$, h^+, and ·OH) generated during the photocatalytic process are responsible for the photocatalytic disinfection. For rhodamine B, a catalytical degradation of 84.2% within 80 min was observed when using a mixture of the unmodified COF and AgI, with most of the catalytic degradation attributed to AgI. However, the performance was increased by the heterojunction formed between the COF and AgI, which enhanced the separation of photogenerated h^+ and e^-, with complete removal within 80 min (Fig. 9bii). On the other hand, 96.3% degradation of acetaminophen was observed when using the unmodified COF, which increased to 97.8% when using a mixture of the unmodified COF and AgI, and was completely removed when employing COF/AgI after 160 min (Fig. 9biii). Although less obvious, the data indicates that the modification of COF-PD with AgI can also enhance the photocatalytic degradation of ACTP.

Amine-rich polymers have also been extensively used in organic dye degradation applications. These commonly include PANI [170], PDA [171], and PPy [172], however others like poly(phenylene sulfide) (PPS) [173] and polythiophene (PTh) [174] have also been evaluated. They have been used for the degradation of methylene orange [175], methylene blue [176], rhodamine B, other dyes [177,178], as well as other pollutants like PVC [179] and phenol [180]. Although amine-rich polymers show effective catalytic activity by themselves [181], many reports combine them with other semiconductor materials to enhance their performance. The most popular involves TiO_2 [182], however other materials like $SrSnO_3$ [183] and $MoSe_2$ [184] have also been reported. As with g-C_3N_4 and COFs, the degradation mechanism relies on photogenerated ROS to break down C-C and C-H bonds of organic pollutants. For instance, $ZnTiO_3$ nanostructures which already possess catalytic properties can be doped with PANI and Ag nanoparticles via a modified sol-gel method to enhance their activity towards environmental remediation applications, specifically methylene blue degradation [185]. When observing the change in absorption spectra for the MB dye molecule in the presence of Ag/PANI/$ZnTiO_3$ under visible light illumination, a decrease in the peaks can be seen, with a flattening of the curve within 25 min (Fig. 9ci). This highlights the effective and target-oriented performance of the photocatalyst. It is important to note that pristine $ZnTiO_3$ showed reduced catalytic performance compared to the hybrid frameworks, whereby 75.8% of the dye was degraded under bare $ZnTiO_3$, 81.7% in the presence of 10%PANI/$ZnTiO_3$, and 95.6% when employing the 1%Ag/10%PANI/$ZnTiO_3$ hybrid nanostructure

(Fig. 9cii). The increased photodegradation performance was attributed to the heterojunction formed between Ag, PANI, and $ZnTiO_3$, which suppressed the high energy requirements for electron-hole pair recombination. This leads to the formation of radicals ($\cdot O_2^-$ and $\cdot OH$) which are highly capable of pollutant degradation. Moreover, the surface plasmon resonance phenomenon of AgNPs in the nanostructure led to the lowering of the band gap energy for the hybrid structures. Ag-based plasmon resonance could capture many visible light photons to redshift the light absorbance, thus enhancing degradation. In combination, these characteristics lead to greatly enhanced photodegradation rates (Fig. 9ciii). Alternatively, amino acid-based hybrid organotitanias can be formed by in situ incorporation of L-tyrosine during synthesis. The crystalline structure, shape, and size can be tuned by varying the pH, resulting in nanoparticles or nanorods at a pH of 2.2 or 0, respectively [186]. The incorporation of L-tyrosine in both morphologies results in a decrease in band gap as well as additional absorption edges at wavelengths higher than 400 nm, allowing for more light absorption in the visible range. As a result, a 2.2x increase in photocatalytic activity is observed compared to the L-tyrosine free titania.

3.2.2. *Pharmaceutical drug degradation*

Pharmaceutical drugs have recently been categorized as an emerging pollutant due to their high consumption, biorefractory nature, and widespread distribution in the environment [187]. Their unrestricted use causes them to be a key contributor towards pollution of surface water, wastewater, and soil, as well as promoting the emergence of antibiotic-resistant bacterial strains [188]. Their stable chemical structure makes them difficult to remove via conventional wastewater

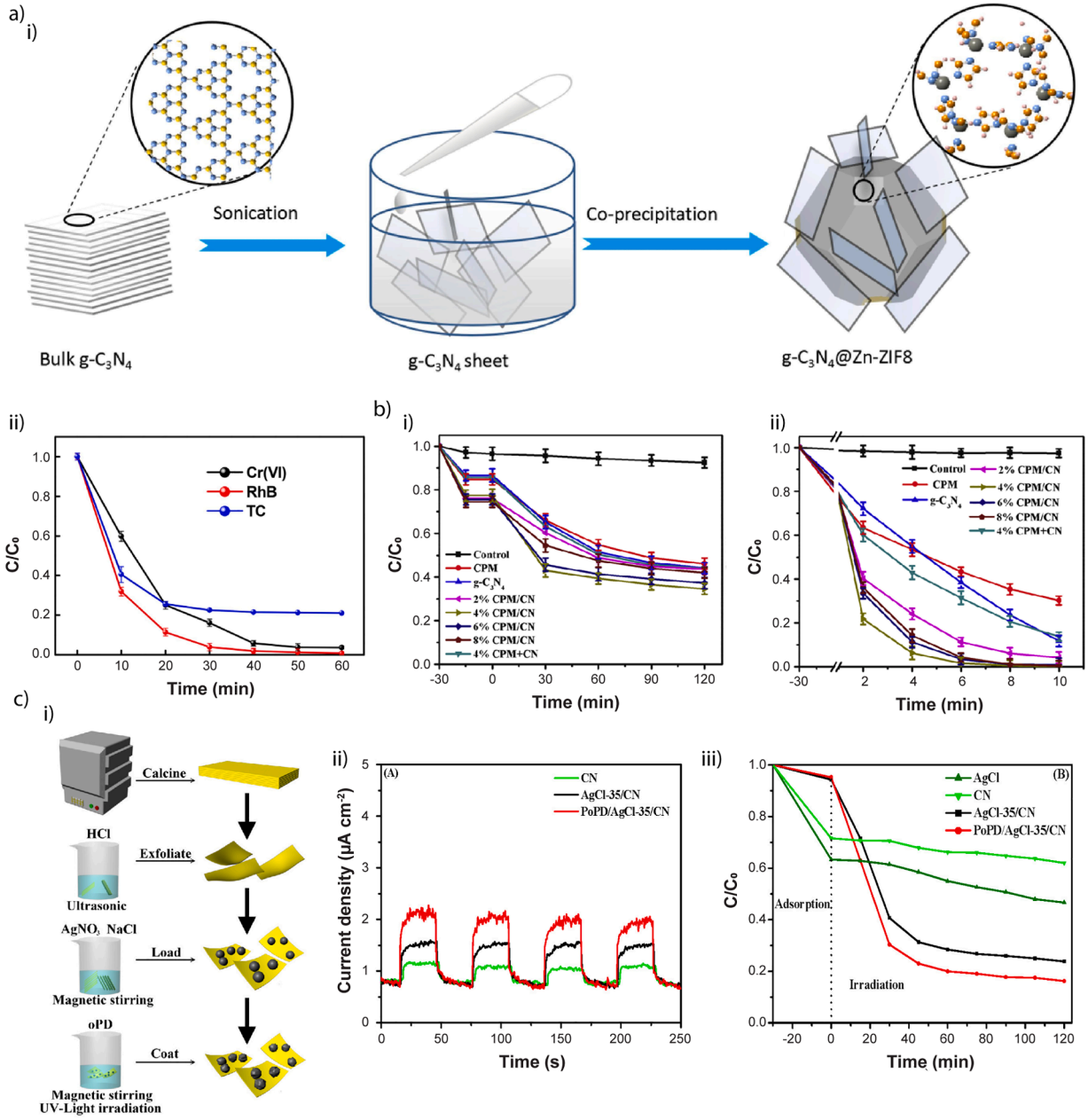


Fig. 10. Catalytic polymeric materials for pharmaceutical drug degradation. a) (i) Schematic illustration of synthesis of g-C_3N_4@ZIF-8. (ii) Photocatalytic degradation of tetracycline, rhodamine B, and Cr(VI) over g-C_3N_4@ZIF-8. Reprinted with permission from [215]. Copyright 2021, Elsevier. b) Photocatalytic degradation of (i) ciprofloxacin and (ii) rhodamine B over a POM/g-C_3N_4 complex. Reprinted with permission from [217]. Copyright 2022, Elsevier. c) (i) Schematic illustration of the synthesis of the PoPD/AgCl/CN photocatalyst. (ii) Transient photocurrent response of CN, AgCl-35/CN, and PoPD/AgCl-35/CN. (iii) Photocatalytic degradation of tetracycline over AgCl, CN, AgCl-35/CN, PoPD/AgCl-35/CN. Reprinted with permission from [221]. Copyright 2019, Elsevier.

treatment options and biodegradation [189], therefore, the residues of the incomplete absorption and metabolism of pharmaceutical drugs can be released into the environment and cause secondary pollution. It is then imperative to develop strategies which can address the impact they have on human health and the environment. Although some polymeric-based platforms have been developed which can degrade drugs including anti-inflammatory [190], anti-convulsant [191], anti-depressant drugs [192], as well as pharmaceutical preservatives [193], the most researched pharmaceutical drugs involve antibiotics [194]. As such, this section will focus on their degradation.

The polymeric platform that has been leading the field in this regard is graphitic carbon nitride, primarily relying on the photocatalytic generation of ROS to degrade them [195]. Tetracycline is the most investigated antibiotic since it is a typical broad-spectrum antibiotic used to prevent human and animal infections and is commonly found in various water bodies [196]. However, the degradation of other antibiotics like ciprofloxacin [197], berberine hydrochloride [198], and ofloxacin [199], among others [200], have also been investigated which rely on similar ROS-generating mechanisms. As with many studies involving this semiconductor-based polymeric catalyst, strategies have been employed which aim to increase their light-absorption capacity and thus increase performance. These include morphology changes [201], heterojunction choice [202], the addition of quantum dots [202] or nanoparticles [203], carbon or nitrogen deficient complexes [204–206], MOF-based composites [207], and various others [208–212]. It is promising to see however, the rise in reports which aim to develop catalysts which can degrade various types of pollutants simultaneously, rather than just one [213]. This is because in many cases, pollutants are synchronous and it is therefore beneficial if they can be removed simultaneously [214]. For instance, MOF-based nanoreactors with photocatalyst inclusion (e.g., g-C_3N_4) can lead to improved performance by enhancing areas of heterojunctions, increasing the amount of active sites, and confining active species within a limited porous space [214]. A core-shelled g-C_3N_4@ZIF-8 photocatalysts with Zn-exposure can be designed with not only enhanced tetracycline degradation compared to pure g-C_3N_4 (4.8 times), but also superior degradation rate of rhodamine B (99.3%) and Cr(VI) (96.6%) (Fig. 10ai-ii) [215]. The photocatalytic activity is due to the synergistic effect that is produced when combining g-C_3N_4 and ZIF-8, resulting in an enhanced transient photocurrent response and a decreased electrochemical impedance spectra than either single material. In other words, the hybrid material exhibits improved carriers' separation and transportation. Similarly, a synergy can be achieved when decorating g-C_3N_4 with polyoxometalates (POM), the latter of which have demonstrated excellent photocatalytic properties [216]. By doing so, a POM/g-C_3N_4 (CPM-CN) complex can exhibit enhanced photocatalytic activity compared to its pure counterparts. This was demonstrated for the degradation of antibiotics (tetracycline and ciprofloxacin) as well as organic dyes (rhodamine B) (Fig. 10b) [217]. As with other platforms, the increased photocatalytic performance was attributed to: (i) the suppressed recombination of photoinduced charge carriers indicating an increased separation ability of electron-hole pairs, thus more effective photocatalytic performance, (ii) a higher transient photocurrent response compared to either single material, indicating a greater photocatalytic behavior as the separation rate of photo-generated electron-hole pairs was enhanced, and (iii) a smaller radius of the arc on the electrochemical impedance spectra suggesting an effective interfacial charge transfer and elevated separation ability of photogenerated electron-hole pairs. A modified carbon nitride framework with a 3:5 C:N stoichiometry can also be developed with a reported narrower bandgap and higher potential of conductive band than that of g-C_3N_4, where the higher N ratio reduces adsorption energy and facilitates electron transfer [218]. This modified carbon nitride can be used to activate peroxymonosulfate (oxidizing agent), which generates ROS and degrades various micropollutants including ciprofloxacin, tetracycline, sulfamethoxazole, and diclofenac sodium [219].

Several studies have also integrated conductive polymers with semiconductors like g-C_3N_4 or TiO_2, enhancing the electrical conductivity, cycle utilization, and electronic transmission rate [220]. In other words, coupling conductive polymers with semiconductors is an effective way to increase photocatalytic activity. For instance, graphitic nanosheets (CN) inherently show improved performance due to their increased specific surface area and reaction sites. However, their catalytic activity can be increased by the incorporation of poly-o-phenylenediamine (PoPD) and AgCl, allowing for 3x the photocurrent density compared to the pure nanosheet (Fig. 10c) [221]. The PoPD/AgCl/CN hybrid exhibits the highest photocurrent density, indicating effective transfer of photogenerated electron-hole pairs (Fig. 10cii), and a smaller radius arc in the impedance curve, indicating lower resistance to charge transfer during the reaction. In combination, these properties can explain the improved photocatalytic activity of the complex, achieving a degradation rate of 74.7% towards tetracycline within 30 min for AgCl-CN and 83.1% for PoPD/AgCl/CN (Fig. 10ciii). Similar catalytic performances were shown for other platforms employing other semiconductors and amine-rich polymers [222,223]. In all cases, the degradation mechanism is attributed to the generation of ROS which degrade the pollutant. Alternatively, nanofiber membranes can be loaded with tungsten oxide (WO_3) nanoparticles surface coated with PDA, and tested for oil/water separation, photothermal water evaporation, as well as ampicillin degradation [224]. For the latter case, the inherent photocatalytic activity of WO_3 was enhanced by the addition of a thin layer of PDA, generating radicals more efficiently and allowing for the degradation of the pollutant. Although this catalyst showed high performance towards oil/water separation and water evaporation, only 40% ampicillin was reduced after 3 h. However, the platform could be improved by fine-tuning the absorption wavelength of the nanocomposite, increasing the loading and exposure of WO_3 on the surface, optimizing the initial concentration of the ampicillin, adjusting the pH, and removing the interfering radical scavengers.

3.2.3. *Toxic gas removal*

The relationship between increased standard of living and pollution is complex and multivariable. On the one hand, it leads to an increased awareness of environmental issues and willingness to reduce pollution and invest in "cleaner" alternatives [225]. On the other hand, it results in increased industrialization, urbanization, and consumption of goods and services, in other words, more energy consumed, waste generated, and pollutants emitted into the environment. An example of this is the increase in motor vehicles which release harmful gasses to the environment and cause severe air pollution [226]. One of these gasses include nitrogen oxides (NOx), with nitrogen oxide (NO) accounting for 90% of NOx in ambient air [227]. Several efficient de-NOx methods including biological [228], chemical [229], photochemical [230], electrochemical [231], and photocatalytic have been developed [232]. The latter approach is currently considered the most attractive due to its cost-effective, simple, and environmentally friendly nature [233]. As expected, polymer-based photocatalytic platforms have also been evaluated to remove NO from air, with the most common examples utilizing g-C_3N_4 and COFs. The mechanism for photocatalytic degradation of NO relies on the generation of ROS [234] and is commonly improved via various strategies such as using different stoichiometric ratios of C:N [235], the addition of natural minerals [236] or their oxides [237], developing models with N-defects [238], as well as different types of heterojunctions [239,240]. For instance, a N-deficient mesoporous carbon nitride can be synthesized with a greater number of exposed active sites, resulting in a wider band gap, thus enhanced redox ability [241]. The N defects create catalytic active sites and induce effective separation of photogenerated carriers. This synergistic effect results in the generation of more ROS, achieving 60.6% higher activity compared to its pure counterpart (g-C_3N_4). Alternatively, K- and B-doped platforms have also been developed with the aim of improving the recombination of photogenerated carriers and low concentration of oxidizing species

[242]. B is introduced by replacing C atoms, while K is inserted into the interlayer by binding to the N and C atoms of adjacent layers. This results in increased electron delocalization and expands the π-conjugate system. As such, expanded light absorption and a reduced band gap can be achieved. This leads to a system 2x more efficient compared to an un-doped variant which can be re-used even after 5 cycles and be used for hydrogen evolution. Interestingly photocatalytic paints containing a PANI/TiO_2 composite have also been developed [243]. The band gap of this composite is decreased compared to TiO_2, whilst showing an increased optical responsivity. These paints showed a 50% decrement in benzene removal under UV light, which increased by 23% under VIS light. It is worth noting that although PANI itself was able to remove benzene under both UV and VIS light, the performance was decreased comparatively.

3.3. *Energy-based applications*

More than two-thirds of worldwide energy demands are currently

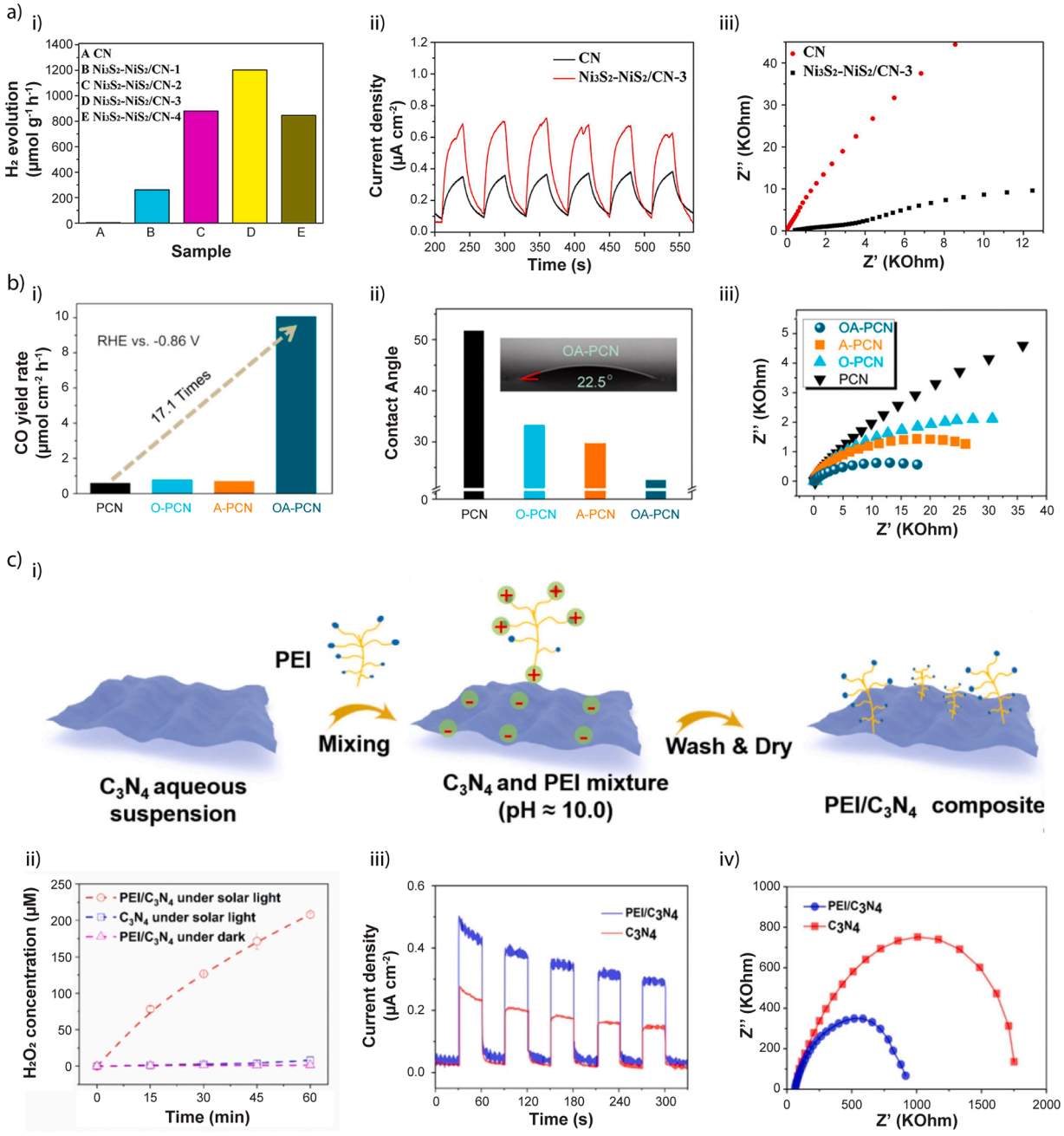


Fig. 11. Catalytic polymeric materials for energy generation. a) (i) H_2 generation rate of g-C_3N_4 (CN) and Ni_3S_2-NiS_2/CN with different loading amount of Ni_3S_2-NiS_2. (ii) Photocurrent density of CN and Ni_3S_2-NiS_2/CN-3, with the higher density implying a superior charge transfer efficiency. (iii) Electrochemical impedance spectroscopy of CN and Ni_3S_2-NiS_2/CN-3, with the smaller radius indicating faster electron transfer. Reprinted with permission from [266]. Copyright 2022, Elsevier. b) (i) CO production rates of PCN, O-PCN, A-PCN, and OA-PCN depicting a ~17x increase for OA-PCN. (ii) Contact-angle measurements and (iii) electrochemical impedance spectroscopy reinforcing the enhanced electron and mass transfer of the polymeric carbon nitride modified with hydroxyl and amino groups on its surface. Reprinted with permission from [300]. Copyright 2019, American Chemical Society. c) (i) Illustration of the functionalization of C_3N_4 nanosheets via an electrostatic assembly process. (ii) H_2O_2 production by PEI/C_3N_4 and C_3N_4. (iii) Photocurrent density of PEI/C_3N_4 and C_3N_4, with the higher density implying a superior charge transfer efficiency. (iv) Electrochemical impedance spectroscopy of PEI/C_3N_4 and C_3N_4, with the smaller radius indicating faster electron transfer for the modified polymer material. Reprinted with permission from [314]. Copyright 2020, American Chemical Society.

met by non-renewable energy sources [244], therefore, great efforts have been placed to transition towards more sustainable energy alternatives. Polymeric catalysts can play a significant role in addressing this issue, mainly via energy generation [245], conversion [246], and storage [247]. The following section will briefly discuss the role of polymeric catalysts in these areas.

3.3.1. Energy generation

3.3.1.1. Hydrogen evolution. Hydrogen (H_2) has emerged as an alternative fuel option to transition the energy industry away from fossil fuels and promote decarbonization. Currently, 85% of H_2 is produced from fossil fuels, however solar-driven polymeric catalysts can be used to generate H_2 in a sustainable manner [248]. g-C_3N_4 is a prime polymeric example that has been extensively evaluated for this application. Various strategies have been employed to increase the photocatalytic H_2 generation from g-C_3N_4. These include different types of heterojunctions such as type-II [249], Z-scheme [250], S-scheme [251], and Schottky heterojunctions [252], metal [253] and non-metal [254] doping, the use of cocatalysts [255], as well as morphology (0D, 1D, 2D, 3D) [256–260] and composition changes [261,262]. In all cases, the primary goal is to overcome some of the limitations of pristine g-C_3N_4 and generate more H_2 comparatively. These improvements can range from a 1–2x increase in H_2 generation [263,264], to up to triple digit increases [265]. For instance, binary Ni_3S_2-NiS_2 can be *in-situ* grown on g-C_3N_4 (CN) to achieve hydrogen evolution efficiencies 300x that of pure g-C_3N_4 (Fig. 11ai) [266]. In this case, the increase is attributed to the faster photogenerated charge separation, as characterized by the photocurrent response curve (Fig. 11aii). The photocurrent density is higher for the complex compared to pristine CN, implying superior charge transfer efficiency. Furthermore, the electrochemical impedance spectra showed a smaller radius for Ni_3S_2-NiS_2 indicating faster electron transfer (Fig. 11aiii). These properties, in conjunction with the increased light absorption capacity of the complex, explain the enhanced hydrogen evolution performance of the catalyst. COFs are also recognized as a promising crystalline porous organic material for photocatalytic H_2 generation. As with g-C_3N_4, several strategies have been employed to improve H_2 evolution, mainly involving functional building blocks and linkages [267,268], heterojunction choice [269], metal-doping [270], and even by developing graphene-like COFs [271]. These improve their electron-deficiency, π-conjugation, or nitrogen/metal-containing catalytic active sites. Furthermore, the type and dispersion of cocatalysts within COFs has also been evaluated to enhance H_2 generation. For instance, adsorption sites for platinum species can be constructed by introducing adjacent hydroxyl group and imine-N within a COF structural unit, leading to the in situ reduction of adsorbed platinum species into metal clusters [272]. The well-dispersed deposition allows for optimal utilization of the Pt co-catalyst, leading to high hydrogen evolution rates. Other polymeric catalysts have also been investigated which aim to improve effective separation, transport, and tunneling of charge carriers. For example, the H_2 generation of pure zinc sulfide (ZnS) can be improved by coating with ultrathin polydopamine, without compromising stability and activity [273]. The improved performance arises from the effective separation, transport, and tunneling of charge carriers of the complex. Moreover, the polydopamine layer improves the wettability of the catalyst while also providing a passivating layer. Additionally, other amine-rich polymers can be incorporated onto semiconductors to increase their performance like PANI, PPy, or PEDOT [273–275]. For instance, the surface of rGO can be functionalized with TiO_2 and attached on polymerized aniline to obtain a catalyst with efficient charge separation [276]. This is because it shows a narrower bandgap energy, increased light absorption in the visible range, rapid photoinduced charge separation, and suppressed charge recombination. Consequently, a H_2 evolution rate of 1.8x greater than TiO_2/rGO and TiO_2 can be obtained.

3.3.1.2. O_2 evolution. It is possible to alter the band structure of g-C_3N_4 to make it more effective towards O_2 evolution reactions [277]. For instance, calcining it with sodium borohydride results in a boron-doped and nitrogen-deficient g-C_3N_4 [278]. This leads to the conduction and valence band being tuned to enable an increase in optical absorption in visible light and driving force for water oxidation, resulting in a 6x increase in O_2 evolution compared to pristine carbon nitride [279]. Similarly, a g-C_3N_4/bismuth vanadate composite can be doped with sulfur to facilitate charge separation and enhance water oxidation [280]. This is because sulfur doping narrows the band gap of g-C_3N_4 by changing the band structure via staking of 2p orbitals on the valence band. The complex exhibits an oxygen evolution rate under visible light irradiation which is 129% greater compared to that of pristine bismuth. Microporous conjugated polymers (CMPs) can also photoelectrochemically generate O_2 from water via doping. By using metal-free pyrene-based nitrogen and sulfur containing CMPs, a low bandgap is achieved, which allows for highly efficient catalytic activity [281]. This increased activity is attributed to the pyrene units in the π-conjugated polymer skeleton, the heteroatoms N and S, as well as the high specific surface area with inherent microporosity. Water splitting to produce hydrogen and oxygen simultaneously is difficult to achieve given that the band-edges of photocatalysts must allow for both water reduction and oxidation for H_2 and O_2, respectively [282]. In other words, a catalyst with suitable band alignments is required which has a conduction band (CB) minimum more negative than the H^+/H_2 energy level, and a valance band (VB) maximum more positive than the O_2/H_2O energy level [283]. A way of achieving this could be by introducing cobalt phosphate ($Co_3(PO_4)_2$) within g-C_3N_4 nanosheets, which could allow for H_2 and O_2 evolution without the need for a cocatalyst. A similar platform was recently demonstrated for a type-II heterojunction photocatalyst based on $Co_3(PO_4)_2$ and reduced graphene oxide (rGO) [284]. In this case, CB or VB edges of rGO and $Co_3(PO_4)_2$ had sufficient overpotential for water reduction or oxidation. Moreover, the formation of a type-II staggered band heterojunction with RGO promoted charge collection and transport, resulting in increased catalytic activity.

3.3.1.3. CO_2 reduction. With the increasing concerns regarding greenhouse gas emissions, specifically CO_2, many strategies have been employed to address this issue, one of which involves carbon capture and utilization (CCU). CCU is the process by which CO_2 emissions are used as a resource rather than released into the environment, thereby mitigating the greenhouse gas effect [285]. As with H_2 and O_2 evolution, a highly researched polymeric catalyst involves g-C_3N_4, which can carry out the catalytic reduction of CO_2 to various hydrocarbons [286], most commonly CH_3OH [287], CH_4 [288], HCOOH [289], and CO [290]. However, due to its poor ability to activate the C-O bond, strategies including doping [291], cocatalyst loading [292], different heterojunctions [293,294], morphologies [295,296], and others [297,298], have been used to improve the catalytic performance [299]. Some strategies have even relied on activating polymeric carbon nitride (PCN) by modifying its surface with hydroxyl (O) and amino (A) groups [300]. These superficial functional groups synergistically activate g-C_3N_4 for CO_2 electroreduction, achieving CO production rates 17x greater compared to the unmodified polymer (Fig. 11bi). In this platform, the surface contact angle of O-PCN, A-PCN, and OA-PCN decreased compared to that of PCN, suggesting the -OH and -NH_2 functional groups could reinforce water adsorption (Fig. 11bii). Moreover, the electrochemical impedance spectroscopy displayed a smaller radius for OA-PCN compared to PCN, implying decreased charge transfer resistance when functionalised (Fig. 11biii). Simultaneously, these properties suggest hydroxyl and amino groups can promote electron and mass transfer, thus enhancing catalytic performance. Similarly, COFs can also be used for CCU, specifically via photocatalytic [301], electrocatalytic [302], or photo-electrocatalytic [303] CO_2 reduction, to generate CO [304], HCHO [305], HCOOH [306], CH_4 [307], as well as C1-C3

chemicals [303]. Most reports rely on hybrid materials, e.g. combining with metals [308] to generate higher yields. However, it is also possible to enhance their catalytic activity by increasing their available active sites via porous three-dimensional (3D) designs which have spatially separated building blocks [309].

3.3.1.4. Other fuels. Alternative strategies for fuel generation have also been evaluated to transition away from fossil-fuels. Another promising liquid fuel involves hydrogen peroxide (H_2O_2), which has also been extensively evaluated [310,311]. Due to the typical low yields of H_2O_2 from water, proton donors can be added to increase catalytic performance, and thus yield [312]. It has also been shown that boron-doped g-C_3N_4 containing nitrogen vacancies can also efficiently catalyze H_2O_2 evolution from water [313]. This is attributed to the effect these variables have on the electronic structure of g-C_3N_4, which leads to different dissociation barriers for the proton donor and promotes the generation of different reactive oxygen species. Similarly, photocatalytic H_2O_2 production can be boosted by the incorporation of PEI (Fig. 11ci-ii) [314]. Briefly, PEI can be grafted onto g-C_3N_4, thereby tuning the local electronic environment. The interaction between PEI and g-C_3N_4 leads to an increase in photocurrent density (Fig. 11ciii) as well as a smaller radius on the Nyquist plot (Fig. 11civ), achieving generation rates 25x higher than pristine g-C_3N_4.

3.3.2. Energy storage

Catalytic polymeric materials have mainly been applied in the field of energy storage to improve power density and stability [315]. Early reports have focussed on lithium-ion batteries, by synergistically promoting electron and ion transmission [316], preventing the formation of an unstable solid electrolyte interphase [317], improving structural stability [318] and storage capacity [319], as well as reducing the activation energy of deposition [320]. More recently, efforts have been placed towards sodium-ion batteries, specifically using catalytic polymers to improve electrochemical reaction processes [321,322]. For instance, annealing g-C_3N_4 at different temperatures results in varying layer spacings, allowing for increased Na^+ storage capacity [323]. This is because annealing affects the content of pyrrole-N, which has a very active p-orbital lone pair. Metal-air batteries have also been receiving significant attention since they use oxygen in the air as a reaction material and are thus an attractive alternative for energy saving and low carbon emissions [324]. By introducing a catalytic polymeric material to the electrode, the charge–discharge capacity/performance, energy efficiency, and cycle stability of the batteries can be improved [325]. For instance, by using single-atom catalysts, such as via the introduction of Pt onto ultrathin g-C_3N_4, the stability and access to multiple active sites can be increased [326]. The single-atom Pt can achieve high dispersibility which increases the utilization efficiency and enhances electrochemical activity. When employed as Li-O_2 batteries' cathode catalyst, Pt/g-C_3N_4 exhibits higher discharge specific capacities compared to pure g-C_3N_4. Alternatively, organo-catalysts like redox-active organic polymers can be developed that enhance diffusion and cycling performance in lithium-ion batteries [327]. To achieve this, triptycene benzoquinone structural units are used to achieve a high density of redox-active sites, while tetramethyl groups provide sufficient steric hindrance to restrict rotation about the C–N imide single bond.

3.3.3. Energy efficiency

In the field of organic chemistry, a great emphasis has been placed on "one-pot" cascade reactions to improve reaction efficiency and minimize material loss from multiple iterations of reaction and purification steps [328]. Catalytic polymeric materials have also been used to tackle this issue, such as in deacetalisation–Henry [329] and deacetalisation–Knoevenagel reactions. For instance, a core-shell microparticle (CSM) can be developed with an acid catalyst (PSSA; polystyrene sulfonic acid) as the core and a base catalyst (VEMAP; 4-N-(4-vinylbenzyl) oxyethyl-N-methylamino-pyridine) as the shell, and be used in a one-pot acid/base-catalysed deacetalisation–Knoevenagel cascade reaction [330]. The CSMs were produced via a two-step surfactant-free emulsion polymerization, without resulting in mutual quenching. These CSMs showed excellent performance in various solvents and recyclability (up to 6 times), whilst also having high potential for scalability. The developed colloidal cascade catalyst could be synthesised on a 25 g scale and produce 10 g of the final product. In fact, some catalytic polymeric materials have shown 100% substrate conversion and yield of the final product such as in the one-pot production of β-nitrostyrene from benzaldehyde dimethyl acetal under cascade reactions (acid-catalyzed deacetalization and base-catalyzed Henry reactions) [331]. To achieve this, microporous polymer supports are modified with ethylenediamine followed by 1,3-propane sultone. This results in the simultaneous immobilization of an acid and base catalyst on a single polymeric support, providing a catalytic synergism. Moreover, the catalyst could easily be recovered via filtration and be reused up to 4 times with approximately 10% loss in performance. Recently, it has also been demonstrated that photocatalytic chromophores can be incorporated into polymeric structural frameworks to allow for covalent heterogenization of a catalyst, specifically towards economical organic synthesis [332]. This class of photoactive organic polymers combines the flexibility of small-molecule dyes with the recyclability of solid-phase catalysts. The active sites within this porous microstructure display an increased reactivity, which is further supported by the mobility of excited states and charged species. This is important as it results in increased stability and catalytic efficiencies. In theory, this approach could allow for any organic or organometallic photocatalyst to be heterogenized through copolymerization with porosity-promoting bulky organic monomers. On the other hand, great efforts have also focussed on the development of catalysts with high potential in sustainable catalysis. CMPs are widely used for heterogeneous Knoevenagel condensation, a strategy for C-C bond formation in organic synthesis [333]. These reactions are usually carried out in harsh conditions like pyridine or sodium ethoxide. However, a Salen-based CMP can be synthesised which can catalyze the Knoevenagel condensation reaction between aromatic aldehyde and malononitrile in a H_2O-ethanol mixture. This solvent is considered more sustainable from an environmental point of view. Moreover, the CMP exhibited excellent thermal stability as well as high porosity, CO_2 uptake, reusability (up to 8 times) and catalytic performance for the cycloaddition of CO_2 with epoxides [334].

4. Concluding remarks

It is not often that materials transcend a single field or function and demonstrate high applicability in a wide range of fields. Within this review, polymer-based catalysts have been shown to be such a material. A focus was placed on studies where polymers themselves performed a catalytic process, or synergistically, in conjunction with other materials, led to enhanced activity. As a result, polymers which met this criterion were predominantly photocatalytic-based, relying on light absorption to create electron-hole pairs that react with absorbed molecules or species in the environment. The performance of photocatalysts are significantly affected by three main areas: (i) light absorption, (ii) separation of photogenerated carriers, and (iii) activation and reaction of reactant molecules. Described and referenced within this review are a plethora of studies which aim to enhance one or more of these steps, with considerable improvements over the last 1–2 decades. However, there are several key areas which could drive the field towards the development of a new generation of catalytic polymers, which will be discussed in this section.

Fundamental understanding: Despite research into these photocatalytic polymers started 1–2 decades ago, their reaction mechanism is still not fully understood. In many cases, researchers outline a range of possible pathways that could be causing the catalytic activity being observed. The lack of fundamental understanding of the reaction

mechanism is severely constraining new design concepts. This is because it becomes difficult to identify the exact area which is limiting the platform. As such, it is important to understand fundamental concepts before continuing forward. This idea was put forward sarcastically in a recent study where bird feces were introduced into graphene to improve electrocatalytic performance [335].

Performance in real samples: Many studies evaluate the activity of their catalyst in pristine conditions rather than environments more closely resembling their intended final use. This could lead to misleading performance indicators, as various contaminants present in "real" samples undergoing the catalytic process could affect activity and recyclability of the platform. This is a key factor which can significantly increase future studies' overall impact and promote industry collaboration opportunities.

Multifunctional catalysts: In line with "real-sample" performance, recently, studies have shown catalysts are able to perform efficient photocatalytic degradation towards various pollutant types. This is an attractive quality as pollutants are commonly synchronous, therefore developing a catalyst which can efficiently degrade various types of contaminants without loss in performance or recyclability is ideal.

Catalyst recyclability/stability: A major focus with all studies reviewed herein is on increasing catalytic activity, either for pollutant degradation, energy generation, or other applications. Although a very important factor, the recyclability of the catalyst, in other words, the ability of a catalyst to be recovered, regenerated, and reused multiple times without significant loss of activity or selectivity, is often overlooked, with many studies evaluating <5 cyclic uses. The catalyst recyclability is highly dependent on the industry and sample, but in all cases has a high impact on costs. As such, demonstrating catalysts can be re-used multiple times with little loss in performance whilst in "real" sample environments would be highly attractive. Furthermore, considering some microbes remain in the environment for extended periods, catalytic stability is another important factor to evaluate.

Large-scale production: With the growing concern regarding sustainable practices, catalyst synthesis should shift towards using more cost-effective strategies and environmentally friendly solvents. This will lead to compounded benefits as a holistic mindset is used which considers all aspects of the catalyst life cycle, especially when considering the previous suggestions.

Other research avenues: Currently, photocatalysis is the main mechanism employed for most polymer-based catalysts. In these cases, light is required to trigger the activity. Other mechanisms which do not require an external trigger could also be investigated. For instance, we have recently demonstrated that amine-rich polymers can efficiently catalytically generate nitric oxide (NO; therapeutic agent) from an endogenous prodrug, GSNO (*S*-nitrosoglutathione) [336]. This means that unmodified polymers can open new avenues for NO-generating materials for various therapeutic applications (antibacterial, antiviral, anticancer, antithrombotic, wound healing, etc.). This largely unexplored diversity of polymer catalysts can be traced back almost 50 years ago, where modified PEI was used to catalyze the decarboxylation of oxalacetate [337]. In fact, some researchers have begun to notice this largely unexplored field and developed polymers with enzyme mimicking qualities by incorporating the hydroxyl group of a serine residue, an imidazole group of a histidine residue, and a carboxyl group of an aspartic acid, onto a polymer scaffold for esterolytic applications [338]. On the other hand, antimicrobial applications for polymer-based catalysts have mainly focussed on bacteria, most likely due to their relatively simple structure and well-developed detection methods. It would then follow that a greater focus be placed on other microbes like fungi and protozoa, as well as other pollutants. This could also provide fundamental understanding of degradation mechanisms. Finally, recent studies have also allowed for the automated synthesis of large libraries of peptides with potential catalytic properties utilizing the unique chemistry and properties of selenium [339].

When taking these improvements into account, polymer-based catalysts have the potential to play a crucial role in tackling the issues currently faced in medicine, environmental remediation, and energy. Considering the rapid development of this field in the last decade, the next generation of catalyst that will tackle many of these mentioned issues are likely to appear soon.

Declaration of Competing Interest

The authors declare that they have no known competing financial interests or personal relationships that could have appeared to influence the work reported in this paper.

Data availability

No data was used for the research described in the article.

Acknowledgments

R.C. acknowledges support from the National Health and Medical Research Council Emerging Leadership Investigator Grant (NHMRC APP1173428) and the UNSW Scientia Fellowship. F.M. acknowledges Angie Davina Tjandra for designing and creating Figs. 1–3.

References

[1] Y.H. Lin, et al., J. Am. Soc. Mass Spectrom. 34 (2023) 109–118.
[2] Allied Market Research, Catalyst Market Statistics, Trends: Industry Analysis 2030. https://www.alliedmarketresearch.com/catalysts-market, 2023 (accessed 22 March 2023).
[3] E. Roduner, Chem. Soc. Rev. 43 (2014) 8226–8239.
[4] A.Z. Fadhel, et al., Molecules 15 (2010) 8400–8424.
[5] C.M. Friend, et al., Acc. Chem. Res. 50 (2017) 517–521.
[6] Y.P. Xue, et al., Chem. Soc. Rev. 47 (2018) 1516–1561.
[7] M. Miceli, et al., Catalysts 11 (2021) 591.
[8] P. Peng, et al., Acc. Chem. Res. 50 (2017) 1171–1183.
[9] Y.M. Lee, et al., Chem. Sci. (2023) 4205–4218.
[10] L. Candish, et al., Chem. Rev. 122 (2022) 2907–2980.
[11] A. Ubaldo-Alarcón, et al., Polymers 14 (2022) 2352.
[12] T.L. Nghiem, et al., Polymers 12 (2020) 2190.
[13] Q. Guo, et al., Adv. Mater. 31 (2019), 1901997.
[14] H. Dong, et al., Int. J. Hydrogen Energy 46 (2021) 32044–32054.
[15] Y. Liu, et al., Mater. Today Energy 31 (2023), 101211.
[16] A. Alaghmandfard, et al., Nanomaterials 12 (2022) 294.
[17] Y. Xing, et al., Chin. Chem. Lett. 32 (2021) 13–20.
[18] S. Gao, et al., Appl. Catal. B: Environ. 295 (2021), 120272.
[19] H. Zhou, et al., Chem 8 (2022) 465–479.
[20] X. Ruan, et al., Chem. Eng. J. 428 (2022), 132579.
[21] L. Ai, et al., Small 17 (2021), 2007523.
[22] P. Yadav, et al., Mater. Adv. 3 (2022) 1432–1458.
[23] Z. Chen, et al., ACS Appl. Mater. Interfaces 13 (2021) 1145–1151.
[24] N. Haque, et al., ACS Appl. Nano Mater. 4 (2021) 7663–7674.
[25] S. Jin et al., InfoMat 4 (2022) e12277.
[26] T. Sick, et al., J. Am. Chem. Soc. 140 (2018) 2085–2092.
[27] L. Ma, et al., Chin. Chem. Lett. 27 (2016) 1383–1394.
[28] R.K. Sharma, et al., Mater. Horiz. 7 (2020) 411–454.
[29] V. Hasija, et al., Coord. Chem. Rev. 452 (2022), 214298.
[30] H. Wang, et al., Chem. Soc. Rev. 49 (2020) 4135–4165.
[31] H.L. Qian, et al., Angew. Chem. Int. Ed. 59 (2020) 17607–17613.
[32] S. Ma, et al., Angew. Chem. Int. Ed. 61 (2022), e202208919.
[33] Y. Xing, et al., ACS Appl. Mater. Interfaces 12 (2020) 51555–51562.
[34] H.S. Xu, et al., Nat. Commun. 11 (2020) 1434.
[35] X. Wang, et al., Nat. Chem. 10 (2018) 1180–1189.
[36] A.I. Cooper, Adv. Mater. 21 (2009) 1291–1295.
[37] S. Kim, et al., ACS Nano 16 (2022) 17041–17048.
[38] S.N. Talapaneni, et al., Chem. Mater. 28 (2016) 4460–4466.
[39] K.Venkata Rao, et al., Phys. Chem. Chem. Phys. 18 (2016) 156–163.
[40] C.A. Wang, et al., RSC Adv. 7 (2017) 408–414.
[41] T.M. Geng, et al., J. Mater. Sci. 51 (2016) 4104–4114.
[42] C. Zhang, et al., Adv. Funct. Mater. 28 (2018), 1705432.
[43] M.E. Elhalwagy, et al., Mater. Today Chem. 27 (2023), 101344.
[44] G.G. Celestino, et al., Environ. Sci. Pollut. Res. 26 (2019) 28444–28454.
[45] L. Zhang, et al., Chemosphere 248 (2020), 126102.
[46] M.R. Abukhadra, et al., Int. J. Biol. Macromol. 173 (2021) 435–444.
[47] S. Senguttuvan, et al., Chemosphere 287 (2022), 132164.
[48] S. Bao, et al., J. Hazard. Mater. 409 (2021), 124470.
[49] Y.R. Lee, et al., Chem. Eng. J. 378 (2019), 122133.
[50] Y. Ma, et al., Sci. Total Environ. 821 (2022), 153453.

[51] S.L. Lee, et al., Polymers 11 (2019) 206.
[52] A. Yadav, et al., Colloid Interface Sci. Commun. 40 (2021), 100339.
[53] K.S. Egorova, et al., Angew. Chem. Int. Ed. 55 (2016) 12150–12162.
[54] Z. Grądzki, et al., Poult. Sci. 99 (2020) 2424–2437.
[55] T.P. Van Boeckel, et al., Science 365 (2019) eaaw1944.
[56] V. Mahmoodi, et al., Environ. Sci. Pollut. Res. 25 (2018) 8268–8285.
[57] A. Kumar, et al., Chem. Eng. J. 382 (2020), 122937.
[58] G.N. Bosio, et al., Photodiagnosis Photodyn. Ther. 37 (2022), 102683.
[59] J.H. Thurston, et al., J. Colloid Interface Sci. 505 (2017) 910–918.
[60] H. Zhang, et al., Rare Metals 41 (2022) 1570–1582.
[61] A. Balapure, et al., ACS Appl. Mater. Interfaces 12 (2020) 21481–21493.
[62] W. Wang, et al., Chem. Eng. J. 378 (2019), 122132.
[63] Y. Yin, et al., Nanoscale 14 (2022) 2686–2695.
[64] H. Liu, et al., Appl. Catal. B: Environ. 261 (2020), 118201.
[65] X. Zeng, et al., Appl. Catal. B: Environ. 274 (2020), 119095.
[66] Y. Cheng, et al., J. Hazard. Mater. 383 (2020), 121166.
[67] L. Wang, et al., Appl. Catal. B: Environ. 325 (2023), 122345.
[68] X. Zhang, et al., Chem. Eng. J. 429 (2022), 132588.
[69] F. Liu, et al., Environ. Sci. Technol. 55 (2021) 5371–5381.
[70] A. Mal, et al., Angew. Chem. Int. Ed. 59 (2020) 8713–8719.
[71] S. Qiao, et al., ACS Appl. Mater. Interfaces 13 (2021) 32058–32066.
[72] F.L. Meng, et al., Talanta 233 (2021), 122536.
[73] T. Liu, et al., J. Photochem. Photobiol. B: Biol. 175 (2017) 156–162.
[74] C. Liu, et al., Chem. Eng. J. 430 (2022), 132663.
[75] Y. Zhang, et al., J. Mater. Chem. B 10 (2022) 3285–3292.
[76] G.P. Yang, et al., ACS Appl. Mater. Interfaces 14 (2022) 28289–28300.
[77] Y. Wang, et al., ACS Appl. Mater. Interfaces 10 (2018) 34878–34885.
[78] Z. Yuan, et al., Small 17 (2021), 2007522.
[79] B. Tao, et al., Chem. Eng. J. 403 (2021), 126182.
[80] D. Han, et al., J. Mater. Sci. Technol. 62 (2021) 83–95.
[81] J. Song, et al., ACS Appl. Mater. Interfaces 12 (2020) 8915–8928.
[82] Q. Zeng, et al., Bioact. Mater. 6 (2021) 2647–2657.
[83] D. Wang, et al., Commun. Mater. 3 (2022) 98.
[84] Y. Xiang, et al., J. Mater. Sci. Technol. 57 (2020) 1–11.
[85] A. Ahmed, et al., Eur. Polym. J. 130 (2020), 109650.
[86] C. Liu, et al., Carbohydr. Polym. 303 (2023), 120436.
[87] B. Sun, et al., Small 18 (2022), 2200895.
[88] P. Li, et al., Compos. B: Eng. 252 (2023), 110506.
[89] Y. Zou, et al., ACS Appl. Mater. Interfaces 14 (2022) 8680–8692.
[90] B. Sun, et al., ACS Appl. Mater. Interfaces 13 (2021) 42396–42410.
[91] H. Elkateb, et al., Int. J. Pharm. 588 (2020), 119794.
[92] Y. Sun, et al., Adv. Mater. 34 (2022), 2109580.
[93] P. Chen, et al., Sci. Adv. 8 (2022) eabl8812.
[94] N.Y. Steinman, et al., Biomacromolecules 22 (2021) 4357–4364.
[95] T. Yadavalli, et al., ACS Infect. Dis. 6 (2020) 2926–2937.
[96] L. Soria-Martinez, et al., J. Am. Chem. Soc. 142 (2020) 5252–5265.
[97] S.C. Günther, et al., Sci. Rep. 10 (2020) 768.
[98] C. Zhang, et al., Chemosphere 208 (2018) 84–92.
[99] V. Hasija, et al., Catalysts 11 (2021) 1448.
[100] N. El-Atab, et al., ACS Nano 14 (2020) 7659–7665.
[101] F. Mazur, et al., Adv. Mater. Technol. 8 (2023), 2201916.
[102] I. Foffa, et al., J. Appl. Biomater. Funct. Mater. 20 (2022), 22808000221076326.
[103] L.G. Ding, et al., J. Mater. Chem. A 10 (2022) 3346–3358.
[104] Y. Li, et al., Water Res. 106 (2016) 249–258.
[105] C. Zhang, et al., Appl. Catal. B: Environ. 248 (2019) 11–21.
[106] R. Cheng, et al., Catalysts 8 (2018) 406.
[107] A.R. Bagheri, et al., Biorg. Med. Chem. 51 (2021), 116493.
[108] Y. Jia, et al., Mater. Sci. Eng. C 117 (2020), 111243.
[109] S. Liu, et al., Macromol. Rapid Commun. 41 (2020), 1900570.
[110] R. Anbazhagan, et al., Mater. Sci. Eng. C 120 (2021), 111704.
[111] S.B. Wang, et al., Biomaterials 234 (2020), 119772.
[112] X. Wan, et al., Chem. Commun. 57 (2021) 6145–6148.
[113] P. Wang, et al., Chem. Sci. 11 (2020) 1299–1306.
[114] F. Shu, et al., J. Nanobiotechnol. 19 (2021) 4.
[115] Z. Mi, et al., J. Am. Chem. Soc. 141 (2019) 14433–14442.
[116] D. Wang, et al., Biomaterials 223 (2019), 119459.
[117] P. Gao, et al., Chem. Sci. 11 (2020) 6882–6888.
[118] K. Wang, et al., ACS Appl. Mater. Interfaces 11 (2019) 39503–39512.
[119] S. Liu, et al., ACS Appl. Mater. Interfaces 12 (2020) 43456–43465.
[120] Q. Guan, et al., ACS Nano 13 (2019) 13304–13316.
[121] C. Hu, et al., Chem. Commun. 55 (2019) 9164–9167.
[122] C. Hu, et al., ACS Appl. Mater. Interfaces 11 (2019) 23072–23082.
[123] H. Taheri, et al., Small 16 (2020), 1904619.
[124] N.S. Heo, et al., Mater. Sci. Eng. C 90 (2018) 531–538.
[125] X. Wu, et al., ACS Appl. Bio Mater. 2 (2019) 1998–2005.
[126] X. Liu, et al., Spectrochim. Acta A Mol. Biomol. Spectrosc. 250 (2021), 119363.
[127] J. Dai, et al., ACS Appl. Mater. Interfaces 11 (2019) 10589–10596.
[128] Y. Wu, et al., Appl. Catal. B: Environ. 269 (2020) 118848.
[129] M. Xu, et al., Chem. Eng. J. 360 (2019) 866–878.
[130] Z. Xu, et al., Inorg. Chem. 61 (2022) 20346–20357.
[131] W. Zhang, et al., Colloids Surf. B. Biointerfaces 199 (2021), 111549.
[132] Y. Yuan, et al., Adv. Mater. 30 (2018), 1800069.
[133] R. Wang, et al., Eur. Polym. J. 110 (2019) 1–8.
[134] L. Wang, et al., J. Hazard. Mater. 444 (2023), 130332.
[135] Y. Chae, et al., Environ. Pollut. 240 (2018) 387–395.
[136] M. Patel, et al., Chem. Rev. 119 (2019) 3510–3673.
[137] V. Kumar, et al., Chemosphere 216 (2019) 449–462.
[138] M. Yu, et al., ACS Appl. Mater. Interfaces 14 (2022) 5376–5383.
[139] C. Sun, et al., Sep. Purif. Technol. 271 (2021), 118873.
[140] Y. Zeng, et al., Chem. Eng. J. 435 (2022), 134918.
[141] X. Zhang, et al., Environ. Sci. Water Res. Technol. 8 (2022) 1965–1975.
[142] Y. Wang, et al., J. Hazard. Mater. 408 (2021), 124818.
[143] C.W. Zheng, et al., Chem. Eng. J. 403 (2021), 126400.
[144] R. Al-Tohamy, et al., Ecotoxicol. Environ. Saf. 231 (2022), 113160.
[145] S. Parmar, et al., Chapter 8 - Microorganism: an ecofriendly tool for waste management and environmental safety, in: M.P. Shah, et al. (Eds.), Development in Wastewater Treatment Research and Processes, Elsevier, 2022, pp. 175–193.
[146] R. Patil, et al., Chapter 8 - Constructed wetland: a promising technology for the treatment of hazardous textile dyes and effluent, in: M. Shah, et al. (Eds.), Development in Wastewater Treatment Research and Processes, Elsevier, 2022, pp. 173–198.
[147] Y. Zhou, et al., Environ. Pollut. 252 (2019) 352–365.
[148] T.S. Anantha Singh, et al., Environ. Eng. Sci. 30 (2013) 333–349.
[149] T.P. Vijayakumar, et al., Diamond Relat. Mater. 121 (2022), 108735.
[150] M. Ding, et al., Chin. Chem. Lett. 31 (2020) 71–76.
[151] I. Rabani, et al., J. Hazard. Mater. 407 (2021), 124360.
[152] J. Wang, et al., J. Phys. Chem. Solids 136 (2020), 109164.
[153] F. Shahsavandi, et al., Appl. Surf. Sci. 585 (2022), 152728.
[154] M. Jourshabani, et al., Chem. Eng. J. 427 (2022), 131710.
[155] H. Cong, et al., ChemistrySelect 6 (2021) 9458–9466.
[156] H. Fattahimoghaddam, et al., J. Hazard. Mater. 403 (2021), 123703.
[157] S. Faryad, et al., Chemosphere 320 (2023), 138002.
[158] Y. Zhang, et al., J. Mater. Chem. A 7 (2019) 16364–16371.
[159] S. He, et al., Appl. Catal. B: Environ. 247 (2019) 49–56.
[160] Y. Hou, et al., Dalton Trans. 48 (2019) 14989–14995.
[161] Y. Yao, et al., J. Colloid Interface Sci. 554 (2019) 376–387.
[162] R.L. Wang, et al., Dalton Trans. 48 (2019) 1051–1059.
[163] H. Xue, et al., Ind. Eng. Chem. Res. 60 (2021) 8687–8695.
[164] Y. Li, et al., ACS Appl. Nano Mater. 2 (2019) 7290–7298.
[165] H. Xue, et al., Green Energy Environ. 8 (2023) 194–199.
[166] K.K. Khaing, et al., Inorg. Chem. 59 (2020) 6942–6952.
[167] T. Bhoyar, et al., ACS Appl. Nano Mater. 6 (2023) 3484–3496.
[168] F. Liu, et al., J. Hazard. Mater. 398 (2020), 122865.
[169] J. Liang, et al., Water Res. 123 (2017) 632–641.
[170] J. Yu, et al., Appl. Surf. Sci. 470 (2019) 84–90.
[171] X. Sun, et al., Colloids Surf. Physicochem. Eng. Aspects 570 (2019) 199–209.
[172] V.E. Podasca, et al., J. Photochem. Photobiol. A: Chem. 371 (2019) 188–195.
[173] C. Yang, et al., Chem. Eng. J. 374 (2019) 1382–1393.
[174] M. Faisal, et al., Mater. Today Commun. 24 (2020), 101048.
[175] R. Tanwar, et al., RSC Adv. 9 (2019) 8977–8993.
[176] S. Saha, et al., Int. Nano Lett. 9 (2019) 127–139.
[177] J. Bhadra, et al., J. Environ. Chem. Eng. 8 (2020), 103746.
[178] M. Mitra, et al., ACS Omega 4 (2019) 1623–1635.
[179] V. Najafi, et al., J. Polym. Environ. 27 (2019) 784–793.
[180] H. Wang, et al., Mater. Lett. 260 (2020), 126906.
[181] B.Haspulat Taymaz, et al., Polym. Bull. 78 (2021) 2849–2865.
[182] Y.J. Lee, et al., Appl. Sci. 10 (2020) 6710.
[183] M. Faisal, et al., Ceram. Int. 45 (2019) 20484–20492.
[184] H. Mittal, et al., Sep. Purif. Technol. 254 (2021), 117508.
[185] M. Faisal, et al., Sep. Purif. Technol. 256 (2021), 117847.
[186] G. Sarigul, et al., Adv. Sustain. Syst. 5 (2021), 2100076.
[187] A. Gogoi, et al., Groundw. Sustain. Dev. 6 (2018) 169–180.
[188] F. Mazur, et al., Nat. Rev. Bioeng. 1 (2023) 180–192.
[189] I.B. Seiple, et al., Nature 533 (2016) 338–345.
[190] Z. Zhao, et al., Chem. Eng. J. 407 (2021), 127167.
[191] Y. Zhou, et al., J. Alloys Compd. 890 (2022), 161786.
[192] J. Luo, et al., J. Colloid Interface Sci. 610 (2022) 280–294.
[193] C. Sandoval, et al., Mater. Res. Bull. 116 (2019) 8–15.
[194] Z. Dong, et al., Chem. Eng. J. 403 (2021), 126383.
[195] X. Li, et al., Chem. Eng. J. 429 (2022), 132130.
[196] J. Guo, et al., Catal. Commun. 122 (2019) 63–67.
[197] M. Yu, et al., Chin. Chem. Lett. 32 (2021) 2155–2158.
[198] Y. Yu, et al., J. Hazard. Mater. 404 (2021), 124171.
[199] Z. Huang, et al., New J. Chem. 46 (2022) 3727–3737.
[200] S. Li, et al., Chem. Eng. J. 382 (2020), 122394.
[201] Y. Wu, et al., J. Hazard. Mater. 414 (2021), 125547.
[202] F. Guo, et al., Sep. Purif. Technol. 210 (2019) 608–615.
[203] D. Jia, et al., Env. Sci. Nano 8 (2021) 415–431.
[204] Q. Shen, et al., J. Hazard. Mater. 413 (2021), 125376.
[205] H. Sun, et al., Chem. Eng. J. 406 (2021), 126844.
[206] J. Jiang, et al., J. Hazard. Mater. 414 (2021), 125528.
[207] Q. Su, et al., Chem. Eng. J. 427 (2022), 131594.
[208] X. Zhang, et al., J. Hazard. Mater. 418 (2021), 126333.
[209] Y. Wang, et al., Ceram. Int. 48 (2022) 2459–2469.
[210] C. Jin, et al., Ind. Eng. Chem. Res. 59 (2020) 2860–2873.
[211] G.Q. Zhao, et al., Colloids Surf. Physicochem. Eng. Aspects 652 (2022), 129870.
[212] K. Ren, et al., Carbon 186 (2022) 355–366.
[213] X. Li, et al., Nano Energy 81 (2021), 105671.
[214] M. Jourshabani, et al., Appl. Catal. B: Environ. 302 (2022), 120839.
[215] X. Yuan, et al., Chem. Eng. J. 416 (2021), 129148.
[216] J. Lan, et al., Nanoscale Adv. 3 (2021) 4646–4658.
[217] H. Shi, et al., J. Solid State Chem. 311 (2022), 123069.

[218] P. Kumar, et al., J. Am. Chem. Soc. 141 (2019) 5415–5436.
[219] J. Zhang, et al., Appl. Catal. B: Environ. 289 (2021), 120023.
[220] X. Yuan, et al., J. Environ. Chem. Eng. 8 (2020), 104178.
[221] L. Sun, et al., Chin. J. Catal. 40 (2019) 80–94.
[222] J. Wang, et al., Mater. Sci. Semicond. Process. 121 (2021), 105329.
[223] L. Ye, et al., Mater. Lett. 236 (2019) 370–373.
[224] M.O. Mavukkandy, et al., Chem. Eng. J. 427 (2022), 131021.
[225] IEA, Global EV Outlook 2022 - Data product. https://www.iea.org/data-and-statistics/data-product/global-ev-outlook-2022, 2023 (accessed 22 March 2023).
[226] H. Wang, et al., ACS Appl. Mater. Interfaces 12 (2020) 40176–40185.
[227] X. Hu, et al., Appl. Surf. Sci. 556 (2021), 149817.
[228] K.A. Brown, et al., Science 352 (2016) 448–450.
[229] A. Eizawa, et al., Nat. Commun. 8 (2017) 14874.
[230] T. Oshikiri, et al., Angew. Chem. Int. Ed. 55 (2016) 3942–3946.
[231] V. Kyriakou, et al., Catal. Today 286 (2017) 2–13.
[232] D. Liu, et al., Small 15 (2019), 1902291.
[233] J. Lasek, et al., J. Photochem. Photobiol. C: Photochem. Rev. 14 (2013) 29–52.
[234] L. Hu, et al., Carbon 200 (2022) 187–198.
[235] J. Zhang, et al., Appl. Catal. B: Environ. 296 (2021), 120372.
[236] X. Li, et al., Environ. Sci. Nano 7 (2020) 1990–1998.
[237] P. Van Viet, et al., J. Materiomics 8 (2022) 1–8.
[238] J. Liao, et al., Chem. Eng. J. 379 (2020), 122282.
[239] Y. Ren, et al., Chin. J. Catal. 42 (2021) 69–77.
[240] M. Fu, et al., J. Alloys Compd. 906 (2022), 164371.
[241] P. Lu, et al., J. Alloys Compd. 934 (2023), 167825.
[242] X. Xia, et al., Langmuir 39 (2023) 1250–1261.
[243] A. Hashemi Monfared, et al., Prog. Org. Coat. 136 (2019), 105257.
[244] IEA, World – World Energy Balances: Overview – Analysis. https://www.iea.org/reports/world-energy-balances-overview/world, 2023 (accessed 22 March 2023).
[245] J. Chen, et al., Appl. Catal. B: Environ. 262 (2020), 118271.
[246] K. Wang, et al., J. Catal. 348 (2017) 168–176.
[247] J.H. Park, et al., Adv. Funct. Mater. 31 (2021), 2101727.
[248] Q. Wang, et al., Molecules 28 (2023) 432.
[249] M. Kombo, et al., Catal. Sci. Technol. 9 (2019) 2196–2202.
[250] W. Lei, et al., Int. J. Hydrogen Energy 47 (2022) 10877–10890.
[251] D.E. Lee, et al., J. Mater. Sci. Technol. 148 (2023) 19–30.
[252] R. Shen, et al., Appl. Catal. B: Environ. 291 (2021), 120104.
[253] H. Zhou, et al., J. Colloid Interface Sci. 610 (2022) 126–135.
[254] L. Acharya, et al., New J. Chem. 46 (2022) 3493–3503.
[255] S. Meng, et al., J. Colloid Interface Sci. 585 (2021) 108–117.
[256] C. Li, et al., Mater. Lett. 308 (2022), 131232.
[257] Z. Mo, et al., Appl. Catal. B: Environ. 225 (2018) 154–161.
[258] Z. Zhao, et al., Langmuir 38 (2022) 11054–11067.
[259] A. Cao, et al., ACS Sustain. Chem. Eng. 7 (2019) 2492–2499.
[260] Q. Li, et al., Chem. Eng. J. 450 (2022), 138010.
[261] J. Li, et al., Carbon 172 (2021) 602–612.
[262] W. Shi, et al., Chem. Eng. J. 382 (2020), 122960.
[263] K. Qi, et al., Chin. J. Catal. 41 (2020) 114–121.
[264] H. Yu, et al., Solar RRL 5 (2021), 2000372.
[265] G. Liang, et al., Appl. Surf. Sci. 504 (2020), 144448.
[266] C. Xi, et al., Mater. Lett. 307 (2022), 131012.
[267] Y. Li, et al., ChemSusChem 15 (2022), e202200901.
[268] Y. Wang, et al., Nat. Commun. 13 (2022) 100.
[269] D. Shang, et al., ACS Sustain. Chem. Eng. 9 (2021) 14238–14248.
[270] J. Chen, et al., Appl. Catal. B: Environ. 241 (2019) 461–470.
[271] J. Xu, et al., Angew. Chem. Int. Ed. 59 (2020) 23845–23853.
[272] Y. Li, et al., Nat. Commun. 13 (2022) 1355.
[273] Y. Kim, et al., Appl. Catal. B: Environ. 280 (2021), 119423.
[274] V.D. Dao, et al., J. Alloys Compd. 775 (2019) 942–949.
[275] H.M. El-Bery, et al., RSC Adv. 11 (2021) 13229–13244.
[276] J. Ma, et al., Renew. Energy 156 (2020) 1008–1018.
[277] S. Chu, et al., ACS Catal. 3 (2013) 912–919.
[278] P. Yang, et al., Appl. Catal. B: Environ. 256 (2019), 117794.
[279] D. Zhao, et al., Adv. Mater. 31 (2019), 1903545.
[280] H.J. Kong, et al., Chem. Mater. 28 (2016) 1318–1324.
[281] S.K. Das, et al., Front. Chem. 9 (2021) 803860.
[282] X. Chen, et al., Chem. Rev. 110 (2010) 6503–6570.
[283] S. Cao, et al., Trends Chem. 2 (2020) 57–70.
[284] A. Samal, et al., ChemSusChem 9 (2016) 3150–3160.
[285] L. Ran, et al., J. Am. Chem. Soc. 144 (2022) 17097–17109.
[286] Z. Zhu, et al., J. Chin. Chem. Soc. 67 (2020) 1654–1660.
[287] P. Madhusudan, et al., Appl. Catal. B: Environ. 282 (2021), 119600.
[288] R.R. Ikreedeegh, et al., J. Environ. Chem. Eng. 9 (2021), 105600.
[289] S. Kumar, et al., J. Photochem. Photobiol. A: Chem. 439 (2023), 114591.
[290] X. Jiang, et al., Appl. Catal. B: Environ. 281 (2021), 119473.
[291] Y.N. Gong, et al., Nano Res. 15 (2022) 551–556.
[292] X. Zhang, et al., Appl. Catal. B: Environ. 286 (2021), 119879.
[293] Y. Huo, et al., ACS Appl. Energy Mater. 4 (2021) 956–968.
[294] N. Su, et al., Inorg. Chem. 61 (2022) 15600–15606.
[295] Q. Liu, et al., Nano Energy 77 (2020), 105104.
[296] K. Chen, et al., Chem. Eng. J. 418 (2021), 129476.
[297] H. Li, et al., Chem. Commun. 56 (2020) 5641–5644.
[298] W. Yang, et al., J. Mater. Chem. A 11 (2023) 2225–2232.
[299] Q. Wang, et al., Adv. Fiber Mater. 4 (2022) 342–360.
[300] N. Meng, et al., ACS Catal. 9 (2019) 10983–10989.
[301] Y. Huang, et al., Appl. Catal. B: Environ. 288 (2021), 120001.
[302] Y. Zhao, et al., Appl. Catal. B: Environ. 291 (2021), 119915.
[303] B. Wang, et al., Chem. Eng. J. 396 (2020), 125255.
[304] Z. Fu, et al., Chem. Sci. 11 (2020) 543–550.
[305] I.Hazra Chowdhury, et al., New J. Chem. 44 (2020) 11720–11726.
[306] K. Guo, et al., Chem. Eng. J. 405 (2021), 127011.
[307] M. Liu, et al., Sci. Bull. 66 (2021) 1659–1668.
[308] H. Dong, et al., Appl. Catal. B: Environ. 303 (2022), 120897.
[309] S.Y. Chi, et al., J. Mater. Chem. A 10 (2022) 4653–4659.
[310] Y. Xie, et al., Appl. Catal. B: Environ. 265 (2020), 118581.
[311] H. Zhao, et al., Chem Catal. 2 (2022) 1720–1733.
[312] Y. Kofuji, et al., ChemCatChem 10 (2018) 2070–2077.
[313] J. Luo, et al., Appl. Catal. B: Environ. 301 (2022), 120757.
[314] X. Zeng, et al., ACS Catal. 10 (2020) 3697–3706.
[315] M.C. Kim, et al., J. Power Sources 453 (2020), 227850.
[316] Y. Hou, et al., Nano Energy 8 (2014) 157–164.
[317] X. Li, et al., Adv. Funct. Mater. 25 (2015) 6858–6866.
[318] M. Hankel, et al., J. Phys. Chem. C 119 (2015) 21921–21927.
[319] J. Chen, et al., ACS Nano 11 (2017) 12650–12657.
[320] Z. Zhuang, et al., Sustain. Energy Fuels 5 (2021) 2433–2440.
[321] A. Roy, et al., Batter. Supercaps 4 (2021) 978–988.
[322] M. Huang, et al., Small Structures 2 (2021), 2000085.
[323] J. Liu, et al., Adv. Mater. 31 (2019), 1901261.
[324] C. Liu, et al., ACS Nano 15 (2021) 3309–3319.
[325] C. Wang, et al., J. Mater. Chem. A 7 (2019) 1451–1458.
[326] W. Zhao, et al., J. Colloid Interface Sci. 564 (2020) 28–36.
[327] A. Wang, et al., J. Am. Chem. Soc. 144 (2022) 17198–17208.
[328] T.L. Lohr, et al., Nat. Chem. 7 (2015) 477–482.
[329] X. Wang, et al., Appl. Surf. Sci. 478 (2019) 221–229.
[330] C. Chen, et al., Angew. Chem. Int. Ed. 60 (2021) 237–241.
[331] S. Ghanooni, et al., ACS Omega 7 (2022) 30989–31002.
[332] R.Y. Liu, et al., Nat. Commun. 13 (2022) 2775.
[333] R. Gao, et al., Front. Chem. 9 (2021) 687183.
[334] P. Ju, et al., Catal. Lett. (2022) 2125–2136.
[335] L. Wang, et al., ACS Nano 14 (2020) 21–25.
[336] Z. Luo, et al., Small 19 (2023), 2200502.
[337] W.J. Spetnagel, et al., J. Am. Chem. Soc. 98 (1976) 8199–8204.
[338] A. Bhaskaran, et al., Polymer 225 (2021), 123735.
[339] G. Wu, et al., Nat. Synth. 2 (2023) 515–526.